

Development of a fast readout system for the  
Ge detector array, Hyperball-J

Department of Physics, Faculty of Science,  
Tohoku University

Kenkoh Sugihara

FY2011



## Abstract

We attempt to perform  $\gamma$ -ray spectroscopy of hypernuclei by using a detector system, Hyperball-J, at J-PARC which is located at Tokai village in Ibaraki prefecture. Hyperball-J consists of germanium (Ge) detectors and background (Compton) suppression counters. The Ge detectors are specialized to the hypernuclear  $\gamma$ -ray spectroscopy. All pre-amplifiers in the Ge detectors for Hyperball-J have a low gain and are of transistor reset type because the detectors are exposed to high energy deposit rate from penetration of charged particles. It is predicted that the conventional readout system can not handle Ge detector signals under the maximum beam intensity ( $\sim 10$  MHz). In order to operate Hyperball-J under severe conditions, the new readout system is necessary.

In this research, a fast readout system for Hyperball-J has been developed. The system consists of an interface amplifier and a digital signal processor. The interface amplifier efficiently extracts pulse height of the signal from a pre-amplifier by using a high-pass filter. The filter enables a use of pile-up separation program in the off-line analysis. It reduces the dead time to  $\sim 1 \mu\text{s}$ , equivalent to the charge collection time of the Ge detector. The amplifier reduces the dead time after the reset pulse (from  $\sim 30 \mu\text{s}$  to  $\sim 8 \mu\text{s}$ ) by cutting the signal with a switch when the pre-amplifier resets charges. The amplifier enables the commercially available digital signal processor modules to be used without any modification in hardwares. Behavior of interface amplifiers after reset signal was checked. The observed problems were fed-backed to the modified version for the actual use.

The dead time due to the reset signal was 6 % in the previous experiment, and is predicted to increase to 13 % in the full intensity beam at J-PARC. The developed system achieved a reduction of the dead time to less than 6 % under the full intensity beam, which is comparable to the previous dead time.

# Contents

<b>1</b>	<b>Introduction</b>	<b>1</b>
1.1	Research of the Hypernucleus . . . . .	1
1.2	E13 Experiments at J-PARC . . . . .	4
1.3	Purpose of this thesis . . . . .	5
<b>2</b>	<b>E13 Experimental Conditions</b>	<b>7</b>
2.1	J-PARC . . . . .	7
2.2	Hyperball-J . . . . .	9
2.3	Ge detector for Hyperball-J . . . . .	10
2.4	Readout Flow of the $\gamma$ -ray signal . . . . .	12
2.5	Problems in Performing the Experiment . . . . .	14
2.5.1	Characteristics of Shaping Amplifiers . . . . .	14
2.5.2	Problems of the Conventional System . . . . .	16
2.6	Solution to the Problems . . . . .	20
2.7	Philosophy of the Development . . . . .	22
2.8	Requirements for the New Readout System . . . . .	23
2.8.1	Sampling-ADC . . . . .	23
2.8.2	The Analog Interface Amplifier . . . . .	25
2.8.3	The Data Transfer . . . . .	28
<b>3</b>	<b>The New Readout System</b>	<b>30</b>
3.1	Selection of Readout Methods . . . . .	30
3.1.1	Waveform readout by a sampling-ADC with ORTEC 671 . . . . .	30
3.1.2	Waveform readout by a sampling-ADC with ORTEC 973U . . . . .	31
3.1.3	Direct readout of the pre-amp output by a DSP . . . . .	32
3.1.4	Differentiation readout of the pre-amp output by a DSP . . . . .	35
3.2	Digital Signal Processing (DSP) Module . . . . .	36
3.2.1	General Properties of the DSP . . . . .	36
3.2.2	DSP Modules . . . . .	39
3.3	Present Status of the System . . . . .	42
3.3.1	Test Measurement with Radioactive Sources . . . . .	42
3.3.2	Points to be Revised . . . . .	45

<b>4</b>	<b>Design of the Interface Amplifier</b>	<b>48</b>
4.1	Factors for Achievement of the Requirements . . . . .	48
4.2	ANL Pick Off Board . . . . .	50
4.3	The interface amplifier for the Tohoku Ge-detector . . . . .	54
4.3.1	The Interface Amplifier for Techno-AP Module . . . . .	54
4.3.2	The Interface Amplifier for GRETINA Module . . . . .	58
4.4	The Operation Check . . . . .	61
4.4.1	The Interface Amplifier for Techno-AP Module . . . . .	61
4.4.2	The Interface Amplifier for GRETINA Module . . . . .	66
<b>5</b>	<b>Future Plan</b>	<b>69</b>
<b>6</b>	<b>Summary</b>	<b>73</b>
<b>7</b>	<b>Acknowledgement</b>	<b>75</b>
<b>A</b>	<b>Sallen-Key Architecture</b>	<b>77</b>
<b>B</b>	<b>Pole-Zero Cancellation Feedback</b>	<b>79</b>
	<b>References</b>	<b>81</b>

# 1 Introduction

Study of the nucleus is one of the most important subjects in physics because matters in nature consists of a nucleus and electrons *i.e.* atoms. Although a nucleus is one part of the "elementary" particle in nature, its properties are not yet well understood. A nucleus is a many body system of nucleons (N) of up to  $\sim 300$ . Therefore, the system is difficult to be described statistically. The forces which bind components of nucleus are strong interaction and electromagnetic interaction and are treated as the nuclear force in the nuclear matter. The information about the properties of the nuclear force has been provided by nucleon-nucleon scattering experiments. In these days, concept of the nuclear force is enlarged to baryon-baryon interactions by including nucleon-hyperon and hyperon-hyperon interactions.

## 1.1 Research of the Hypernucleus

A hypernucleus is a nucleus in which hyperons are bound. Nucleon consists of up and down quarks, and the hyperon contains a strange quark additionally. The hyperon-nucleon (YN) interaction is different from the nucleon-nucleon (NN) interaction. In order to study properties of the nuclear force between a nucleon and a hyperons in low energy region, the traditional particle scattering method ( $\Lambda$ -N scattering) is not valid because of the short or sub-nanosecond lifetime of hyperons. For example, the lifetime of  $\Lambda$  hyperon is  $\tau_\Lambda \sim 263$  ps and that of  $\Sigma$  is  $\tau_\Sigma \sim 80$  ps. Since these lifetimes are longer than that of de-excitation by electromagnetic or strong interaction, the nuclear force of the hypernucleus is mainly studied by measuring hypernuclear level structures.

A schematic low-lying level structure of the hypernucleus is shown in Fig. 1. These energy spaces are dependent on the  $\Lambda$ N interaction and wave-function of the nucleus. The two body interaction in the free space is modified in the many body system, and is treated as the effective interaction. The effective  $\Lambda$ N interaction is given by as follows:

$$V_{\Lambda N}(r) = V_0(r) + V_\sigma(r)\mathbf{s}_N \cdot \mathbf{s}_\Lambda + V_\Lambda(r)\mathbf{l}_{\Lambda N} \cdot \mathbf{s}_\Lambda + V_N(r)\mathbf{l}_{\Lambda N} \cdot \mathbf{s}_N + V_T(r)\mathbf{S}_{12} \quad (1)$$

where the  $\mathbf{S}_{12}$  is written as

$$\mathbf{S}_{12} = 3(\boldsymbol{\sigma}_N \cdot \hat{\mathbf{r}})(\boldsymbol{\sigma}_\Lambda \cdot \hat{\mathbf{r}}) - \boldsymbol{\sigma}_N \cdot \boldsymbol{\sigma}_\Lambda, \quad (2)$$

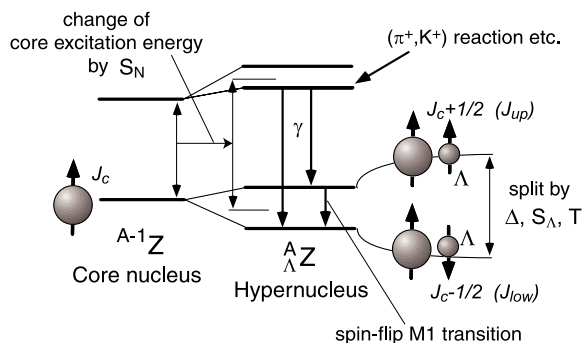


Figure 1: A schematic level structure of the hypernucleus.

$r = |r_\Lambda - r_N|$  is the relative distance between the  $\Lambda$  and the nucleon (N) and  $\mathbf{l}_{\Lambda N}$  is the relative orbital angular momentum. The terms of  $V_0(r)$ ,  $V_\sigma(r)$ ,  $V_\Lambda(r)$ ,  $V_N(r)$  and  $V_T(r)$  are radial potentials of spin-averaged central, the spin-spin, the  $\Lambda$ -spin dependent spin-orbit, the nucleon-spin dependent spin-orbit and the tensor interactions, respectively. The measured values (level schemes) are given by radial integration of the  $V_{\Lambda N}(r)$  with a proper wave function and each integrated values are denoted as  $\bar{V}$ ,  $\Delta$ ,  $S_\Lambda$ ,  $S_N$  and  $T$  in case of p-shell hypernucleus. The parameters of the spin-dependent components,  $\Delta$ ,  $S_\Lambda$ ,  $S_N$  and  $T$ , were determined by the previous experiments at KEK (High Energy Accelerator Research Organization, Japanese name: Kou Energy kasokuki Kenkyuu kikou) and BNL (Brookhaven National Laboratory), where the  $\bar{V}$  contributes equally to all level energies hence not to be considered here. For example,  $\Delta$  is expressed as

$$\Delta = \int dr r^2 \phi_{\Lambda N}^*(r) V_\sigma(r) \phi_{\Lambda N}(r) \quad (3)$$

and determined to be  $\Delta = 0.33$  MeV. The determined parameters are listed in the Table 1.

Level structures are measured by two different methods, one is reaction spectroscopy and another is  $\gamma$ -ray (or decay particle) spectroscopy. The re-

Table 1: The interaction parameters of the  $\Lambda$ -N spin-dependent interaction

Parameter	MeV
$\Delta$	0.33
$S_\Lambda$	-0.01
$S_N$	-0.43
$T$	0.03

action spectroscopy measures the momenta of in-coming and out-going particles. By calculating missing mass of the produced hypernucleus, its energy levels are studied. Although the method is very powerful, energy resolution of the reaction spectroscopy is worse than low-lying excited states (Fig. 1). Even though the resolution of the (e,e'K) experiment which achieved the best resolution in the hypernuclear reaction spectroscopy is several hundred keV, it cannot resolve these spacing. In order to measure the spacings, we have to measure them by other methods.

The  $\gamma$ -ray spectroscopy measures the  $\gamma$  rays from an excited hypernucleus. Since germanium (Ge) detectors have a very high resolution (a few keV for a MeV  $\gamma$  ray), the hypernuclear  $\gamma$ -ray spectroscopy with Ge detectors is now the only way to study the  $\Lambda$  spin-dependent interaction. The above parameters in Table 1 are determined by using this method with the Ge detectors array Hyperball and Hyperball-2. Hypernuclear spectroscopy detects energy level spacings of the bound states because the  $\gamma$  rays are emitted from bound states of the hypernucleus. We are constructing a new Ge detector array called Hyperball-J for further research of hypernuclei and the nucleon-hyperon force. The details of the Ge detectors are described in the section of the E13 experimental conditions.

## 1.2 E13 Experiments at J-PARC

The previous  $\gamma$ -ray spectroscopy experiments with Ge detectors array, Hyperball and Hyperball-2, at KEK and BNL measured light p-shell hypernuclei and determined the parameters in Table 1. We plan to perform the  $\gamma$ -ray spectroscopy of light hypernuclei at J-PARC (Japan Proton Accelerator Research Complex) for further study of hypernuclei. The experiment is named E13. In order to measure  $\gamma$  rays from hypernuclei, we use the Ge-detector array, Hyperball-J.

We will measure  $\gamma$  rays from  ${}^4_{\Lambda}\text{He}$ ,  ${}^{19}_{\Lambda}\text{F}$ ,  ${}^7_{\Lambda}\text{Li}$ ,  ${}^{10}_{\Lambda}\text{B}$  and  ${}^{11}_{\Lambda}\text{B}$ . The main purpose of the E13 experiment is described as follows.

- (1) We plan to further study the  $\Lambda\text{N}$  interaction through level structures of light hypernuclei. For this purpose we study following hypernuclei:
  - (1-1)  ${}^4_{\Lambda}\text{He}$  : For the test of charge symmetry breaking effects in the  $\Lambda\text{N}$  interaction,
  - (1-2)  ${}^{19}_{\Lambda}\text{F}$  : For measuring the strength of the effective  $\Lambda\text{N}$  spin-spin interaction in the sd-shell  $\Lambda$  hypernuclei, which provides information on the radial dependence of the  $\Lambda\text{N}$  interaction,
  - (1-3)  ${}^{10}_{\Lambda}\text{B}$  and  ${}^{11}_{\Lambda}\text{B}$  : For the consistency check of the strengths of the  $\Lambda\text{N}$  spin-dependent interactions parameters.
- (2) We also plan to study modification of baryon properties in a many body system by measuring a reduced transition probability  $B(\text{M}1)$  of  $\Lambda$  spin-flip M1 transition in  ${}^7_{\Lambda}\text{Li}$  to extract a g-factor of a  $\Lambda$  inside a nucleus.

The E13 experiment consists of the two stages. The first part will be performed at the K1.8 beam line, and  $\gamma$  rays from  ${}^4_{\Lambda}\text{He}$  and  ${}^{19}_{\Lambda}\text{F}$  will be measured. In the second part, experiments for the rest of hypernuclei will be performed at the K1.1 beam line. In the following section we discuss the experiment at the K1.8 beam line because technical problems (*e.g.* dead time, noise condition for detecting  $\gamma$ -rays, etc.) are not so different between the two beam lines.

### 1.3 Purpose of this thesis

A new readout system for hypernuclear  $\gamma$ -ray spectroscopy has been designed through this study. This thesis discusses problems for the conventional system under high energy deposit rate condition of the E13 experiment. A new readout method is required to solve the problems and it is found that waveform readout method is feasible for our purpose. Reasons for the use of the waveform readout method are discussed. We chose a digital signal processing (DSP) module for the new readout system. However, the dynamic range of DSP is less than that of our reset type pre-amplifier of the Ge detectors because commercially available DSPs have been designed and used for resistive feedback pre-amplifiers. We modified DSP by attaching an interface amplifier in front of the module in order to achieve a required resolution, namely, 3 keV (full width at half maximum) @ 1.3 MeV  $\gamma$  ray. The use of the interface amplifier achieved the required resolution but also produced a comparable dead time to the conventional system. The dead time has to be reduced for handling under the high energy deposit rate condition. The study boils down to the development of an interface amplifier with little dead time.

These subjects are mainly discussed in following sections:

**Chap. 2** General conditions of the experiments and characteristics of the Ge detectors array, Hyperball-J, are introduced. Problems of the conventional system under the high energy deposit rate condition are studied. Advantage of waveform analysis methods is clarified through the discussion. Requirements for the new readout system are discussed in order for the system to conquer the problems.

**Chap. 3** Total four waveform readout methods are compared. Reasons for the use of digital signal processing (DSP) module are described. Functions of DSP modules are also introduced. A differentiation circuit is inserted for an interface amplifier which attempts to acquire signals of the transistor reset type pre-amplifier with the required resolution. Energy resolution of DSP with the modification, which is the most important for the  $\gamma$ -ray spectroscopy, is examined and it achieved a comparable performance to that of the conventional system. However, a comparable dead time (a few tens micro-seconds) to the conventional system also occurred after the reset signal. The necessity of development of the interface amplifier with fast recovery is clarified.

**Chap. 4** Designs of new interface amplifiers are introduced. Interface amplifiers are designed in order to shorten the dead time after the reset because reduction of the dead time is indispensable for the actual use in the experiments. Reduction of the dead time is attempted by switches. The switch changes processing time of the interface amplifier, and shorten the dead time. The designed interface amplifier is based on the one developed in Argonne National Laboratory (ANL). First and second order differentiation circuits are designed because a filter with higher order is made from combinations of these two filters. The second order filter is entirely new design for the experiment. The function of these amplifiers are briefly introduced in this section. The behavior around the reset signal were checked in this stage. Measured problems are fed-back to the design of the amplifier for the actual use.

**Chap. 5** The final design of the interface amplifier is introduced. The charged particle detection system which reduces dead time after penetration of a charged particle is also implemented in this stage. This function also uses the switches for the reset signal. Packaging of the interface amplifier is also discussed.

## 2 E13 Experimental Conditions

We plan the  $\gamma$ -ray spectroscopy of light hypernuclei at J-PARC. The  $\gamma$  rays from a hypernucleus are measured by Hyperball-J. The technical properties of E13 experiments are briefly explained in the following section, and the problems of the readout system under a high energy deposit rate are also introduced. A new readout system is required in order to solve the problems and validity of waveform readout method is clarified during the discussion.

### 2.1 J-PARC

J-PARC (Japan Proton Accelerator Research Complex) is a high intensity proton accelerator facility. The main aim of the facility is to pursue frontier in material and life science and nuclear and particle physics.

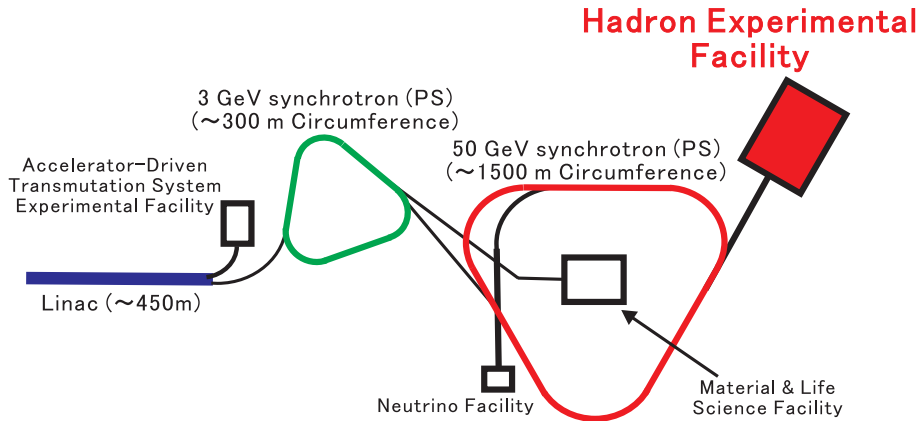


Figure 2: A schematic of the J-PARC.

Figure 2 shows a schematic view of the J-PARC. The J-PARC consists of four experimental facilities, and these are named the accelerator-driven transmutation system experimental facility, the material and life science facility, the neutrino facility and the hadron experimental facility, respectively. The linac (blue line) accelerates  $H^-$  ions to 400 MeV (50 mA), and  $H^-$ s are converted to protons ( $H^+$ ) at the entrance of the 3 GeV Rapid-Cycling Synchrotron (RCS, green line). RCS accelerates protons to 3 GeV ( $333 \mu A$ ) and

then at Main Ring (MR, red line), up to 50 GeV ( $15 \mu\text{A}$ ). At the first phase of the development of the accelerator, MR accelerates beam up to 30 GeV ( $9 \mu\text{A}$ ). The proton beam in MR is transported to the hadron facility and the secondary hadronic beam is produced for experiments. The intensity of the hadronic beam is up to 10 MHz at 50 GeV, and 2 MHz at 30 GeV.

The K1.8 beam line at which we plan to perform the first stage of the E13 experiment is shown in Fig. 3. The proton beam from MR is converted to

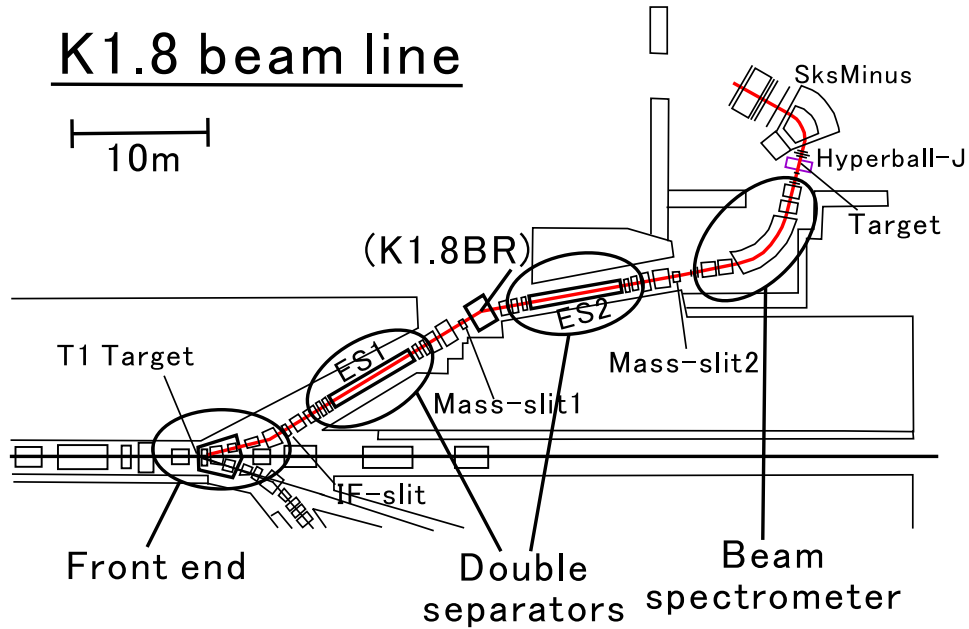


Figure 3: K1.8 beam line.

the secondary hadronic beam at the T1 target (Platinum). The reaction for producing  $\Lambda$  hypernuclei is  $(K^-, \pi^-)$ , and hence kaons have to be extracted from the secondary beam. The double separators (ES1,2 and Mass-slit1,2) extract  $K^-$ . The designed  $K^-/\pi^-$  ratio is 6.9 @ 1.8 GeV/c and 2.5 @ 1.5 GeV/c. The beam spectrometer measures the momentums and trajectories of the in-coming particles and detects Kaons. An in-coming kaon interacts with a nucleus in the target, and a  $\Lambda$  hypernucleus is produced. The momentum and trajectory of an out-going pion from the target are measured by the spectrometer system called SKS-minus. SKS-minus consists with the

SKS (Superconducting Kaon Spectrometer) dipole magnet and other particle detectors. The trigger for  $(K^-, \pi^-)$  reaction is generated by using the beam spectrometer and the SKS-minus spectrometer. Hyperball-J surrounds a target and measures  $\gamma$  rays from a  $\Lambda$  hypernucleus.

## 2.2 Hyperball-J

Hyperball-J is Germanium (Ge) detectors array which specializes to measure  $\gamma$  rays from a  $\Lambda$  hypernucleus. Figure 4 shows the lower half of Hyperball-J. Every Ge detector is a N-type semiconductor and has a 60 % relative detec-

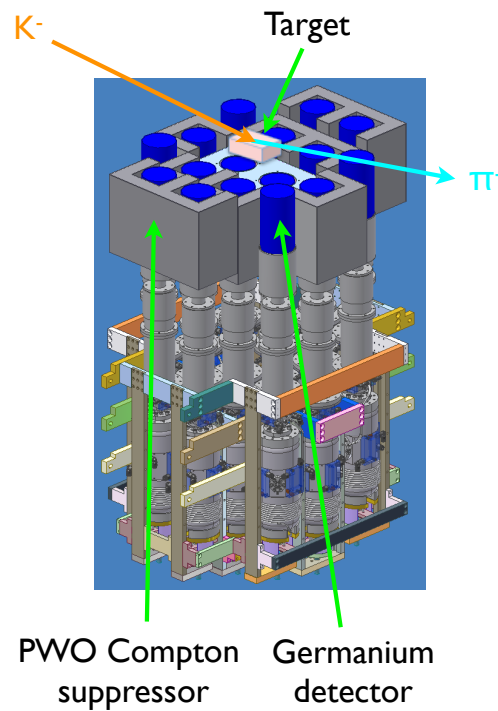


Figure 4: Half side (the downer half) of the Hyperball-J.

tion efficiency. A total of 32 Ge detectors is installed in the array. The major properties of Hyperball-J are as follows:

- The wall type configuration increases solid angle from the target and makes the photo peak efficiency be  $\sim 6\%$  at 1.3 MeV, which is 1.5 times of that of Hyperball 2.
- A pulse tube cooling machine enables the Ge detector to be cooled down to less than 85 K, and delays worsening of an energy resolution due to the radiation damage on Ge crystals.
- The use of PWO ( $\text{PbWO}_4$ ) counter as a background (Compton) suppressor makes the system operate under a higher count rate than that of a BGO ( $\text{Bi}_{12}\text{GeO}_{20}$ ) counter.
- The use of a new readout system for the Ge detector reduces dead time less than the conventional system.

The development of above three items have been completed, and the last one is the under development. Hosomi has researched on the readout system and showed a feasibility of a waveform readout method in the earlier work. In this thesis, a further study on the last item is described.

### 2.3 Ge detector for Hyperball-J

Germanium detector is classified as a semiconductor detector. An important property of Ge detector is a very small energy gap ( $\sim 3$  eV) for the creation of electron-hole pair. The energy resolution of the radiation detector is mainly dependent on the fluctuation of the number of carriers which transport information of energy deposit in the detector. Since the detector which has a smaller energy gap for the pair creation produces the larger number of carriers and reduces the fluctuation, the Ge detector enables precise energy measurements of  $\gamma$  ray. The Ge detector for Hyperball-J has a resolution of 3 keV (FWHM) @ 1.3 MeV. A germanium detector has to be cooled less than 100 K since the small energy gap causes many thermally excited electron-hole pairs, which are source of noise in the signal, at the higher temperature.

The Ge detectors for Hyperball-J have a crystal of  $7\text{cm } \phi \times 7\text{ cm } l$ , which is of a N-type coaxial configuration. Although a Ge detector which is exposed to radiation increases the amount of hole trapping, the trapping is less compared to a P-type detector because the carrier of the N-type is an electron. The collection time of the carrier is roughly estimated to be  $\sim 0.4\ \mu\text{s}$  considering the size of the detector and the drift velocity of the carrier in Ge

( $\sim 10^5$  m/s). This value is important for the design of a pre-amplifier and a shaping amplifier discussed in the following section.

The pre-amplifier (pre-amp.) for Hyperball-J is a transistor reset type. The pre-amp. is installed on the Ge detector. Since in the  $\gamma$ -ray spectroscopy of  $\Lambda$  hypernucleus Ge detector is exposed to a large number of charged particles, the commonly used resistive discharge with a high-gain pre-amp. does not work under the high energy deposit condition. As a matter of fact, one pion penetration deposits  $\sim 70$  MeV in the detector and totally the energy of  $\sim 1$  TeV is deposited per second. In order to handle the pre-amp in the high energy deposit environment, the pre-amp. is designed to accumulate charge which corresponds to the energy of 150 MeV until a reset occurs. The range of 150 MeV/reset corresponds to a few charged particle penetration.

While the energy resolution is one of the most important factor in the  $\gamma$ -ray spectroscopy with a Ge detector. Higher gain achieves good resolution against electric noise. Although the conventional gain of the pre-amp. is  $\sim 100$  mV/MeV, a full range of  $\sim 15$  V is necessary in the case of the Hyperball-J detectors. Considering the voltage supply for the pre-amp. and the technology, the pre-amp. which has a 100 mV/MeV gain and achieves a good resolution is not realistic in case of Hyperball-J. The pre-amp. for Hyperball-J is designed to value operation under the high energy deposit environment and designed to have the gain of  $20 \sim 50$  mV/MeV. The Ge detectors are made by ORTEC (AMETEK, Inc.) and CANBERRA (AREVA SA) and the characteristics of the pre-amps. are listed in Table 2.

Table 2: The characteristics of a Ge detector for Hyperball-J

Property	ORTEC	CANBERRA
Gain	$\sim 50$ mV/MeV	$\sim 30$ mV/MeV
Polarity	Negative	Positive
Range	$-6$ V	$+3$ V
Reset length	$4 \mu$ s	$2 \mu$ s
Reset trigger type	TTL	TTL
Number of detectors	24	8

## 2.4 Readout Flow of the $\gamma$ -ray signal

The trigger for the  $\gamma$ -rays detection from a  $\Lambda$  hypernucleus is the coincidence of detection of an in-coming kaon and an out-going pion. Each trigger is made by the beam spectrometer and the SKS-minus, respectively.

The coincidence between the two spectrometer systems is called to  $(K^-, \pi^-)$  trigger. The  $(K^-, \pi^-)$  trigger signals a production of a  $\Lambda$  and sets the data acquisition system (DAQ) to be ready for an acquisition of the  $\gamma$ -rays data. A logic signal for the  $(K^-, \pi^-)$  trigger needs a short time interval of less than a few hundred nano seconds. Additionally, contaminating particles have to be eliminated. For these reasons scintillation counters and the Cherenkov counters are used for the online trigger. Data of drift chambers for the particle trajectory and momentum study (by off-line) are recorded.

A  $\gamma$  ray which interacts with a Ge detector is converted into an electric signal and collected in a capacitor in the pre-amp over  $0.4 \mu\text{s}$  mentioned above. The collection time is  $0.4 \mu\text{s} \sim 1.2 \mu\text{s}$  empirically. A signal from the pre-amp. is converted by using a shaping-amplifier into a readable shape by an analog to digital converters (ADC). The conventional shaping amplifier (shaping-amp) is ORTEC 973U, an ultra high rate amplifier. ORTEC 671 semi-gaussian shaping-amp. is also used for performance evaluation of Ge detectors under low counting rate. Figure 5 shows schematic view of a signal

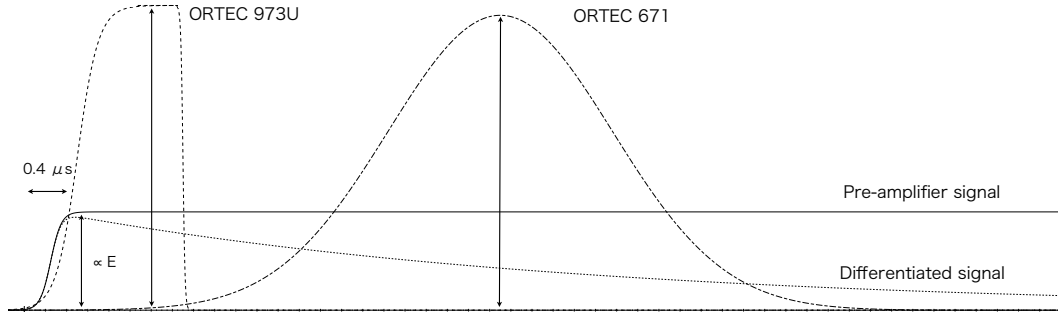


Figure 5: Schematic view of input signal (solid line), differentiated signal inside a shaping-amp. (shorter dotted line) and output of ORTEC 671 shaping-amp. (dashed line) and ORTEC 973U (longer dotted line). The step and the pulse heights correspond to energy (E) deposit inside the Ge detector.

of pre-amp. (solid line) and output of shaping-amp. (dashed line) in case of

the semi-gaussian shaping and one of ultra high rate amplifier (longer dotted line). The shaping-amps. firstly differentiates the input signal (shorter dotted line in Fig. 5) to extract difference of a step, which corresponds to energy deposit in the detector. The differentiated signal is processed into output shapes (dashed line and longer dotted line) by proper filters. The pulse height of the outputs is related to the energy information. Although the semi-gaussian shaping-amp. processes much longer time interval than the width of the step, ORTEC 973U processes  $3 \mu s$  to reduce dead time with a special processing method described below (Fig. 7). In case of secondary  $\gamma$ -ray being detected during the processing time, such events are rejected by the pile up reject function (PUR).

A conventional readout system for  $\gamma$ -ray signal is drawn in Fig. 6. Signal

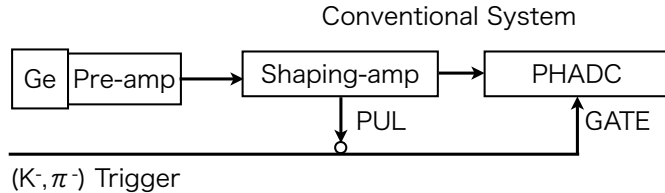


Figure 6: A diagram of the readout system of a Ge signal.

form a pre-amplifier is processed by ORTEC 973U, ultra high rate amplifier and then the signal height is acquired by AD413A (ORTEC), peak hold ADC (PHADC). AD413A acquires the highest position of input pulse. The ADC is controlled by FERA (Fast Encoding and Readout ADC) standards. The first stage of the E13 experiment is also performed by using this system.

A background suppressor (Compton suppressor) rejects an event in which a  $\gamma$  ray is scattered by the Compton scattering with an electron and goes out of the Ge detector. Since veto signals for the Compton event need a short time interval in order to reduce dead time, PWO counters are used for the background counter and surround Ge detectors (Fig. 4). The pulse width of the PWO ( $PbWO_4$ ) counter is  $\sim 50$  ns, on the other hand, that of BGO ( $Bi_{12}GeO_{20}$ ) counters, which were used in the previous systems Hyperball and Hyperball-2, flashes in  $\sim 1 \mu s$ .

Events which satisfy the above condition *i.e.* ( $K^-, \pi^-$ ) reaction are acquired by the DAQ system. A data set mainly consist of not only energy

information of Ge detectors and trajectory detectors but also timing information of the detectors and the counters.

## 2.5 Problems in Performing the Experiment

The ordinary  $\gamma$ -ray experiments are performed under a low energy deposit rate and a low background environment. The experiments values acquisition with a higher resolution. The collection time of careers takes a few  $\mu\text{s}$  and the processing time of the shaping-amp. takes a few tens of  $\mu\text{s}$  order. However a readout system for the hypernuclear  $\gamma$ -ray spectroscopy have to be designed to perform in a high energy deposit rate condition. The conventional fast readout system gets to reach the performance limit and is no more feasible in the full intensity beam at J-PARC. In this section, characteristics and problems of the system are introduced and then a solution is discussed.

### 2.5.1 Characteristics of Shaping Amplifiers

The ORTEC 671 shaping-amp. is used for the ordinary  $\gamma$ -ray spectroscopy and the detector test under low count rate in our laboratory. The shaping amplifier achieves the best resolution over 6  $\mu\text{s}$  shaping time with the Ge detector for the Hyperball-J. The amplifier takes very long time to process an input signal with a semi-gaussian shaping amplifier. Reason of the long processing time is understood as follows: The amplifier processes an input as a step function with zero rise time. The output signal is expressed by the convolution of the step response of the shaping-amp. and the input signal. Shape of output signal is changed by that of the input signal. Although difference of the step is considered to be energy deposit in the Ge detector (Fig. 5), the pulse height of shaping-amp. is not relative to the energy in case of comparable shaping time to the rise time of the pre-amplifier. In this case the surface of the pulse is relative to the difference of the step and hence peak sensitive ADC cannot be used. On the other hand, if time scale of the step response is much larger than that of the input signal, the input signal is approximated to be a step function. In this case, fluctuation of the charge collection time can be negligible and the output pulse height is relative to the energy information.

A pulse width of an output signal is about six times of the shaping time. In case of a 6- $\mu\text{s}$  setting with gaussian pulse shaping, the pulse width is 32  $\mu\text{s}$  (Table 3). The relations between shaping time and energy resolution at

1.3 MeV, a pulse width and a reset pulse width which is discussed below are listed in Table 3. However, experimental conditions for  $\gamma$ -ray spectroscopy

Table 3: The characteristics of ORTEC 671 shaping amplifier

Shaping time [ $\mu$ s]	0.5	1.0	2.0	3.0	6.0	10
FWHM (@1.3 MeV) [keV]	11.4	4.0	2.7	2.6	2.4	2.4
Pulse width [ $\mu$ s]	3.0	5.3	11	16	32	49
Reset pulse width [ $\mu$ s]	7.0	11	19	27	53	83

of  $\Lambda$  hypernucleus are of a high background environment and it is difficult to take a long time for a signal processing. The art of reducing the reshaping time as short as possible is desired for the operation of the experiment.

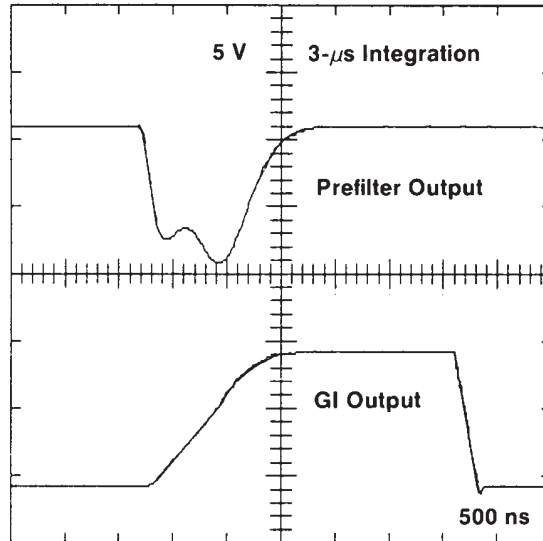


Figure 7: The signals of the ORTEC 973U ultra high rate amplifier. (Top) The internal processing signal which has two humps. (Bottom) The output signal of the 973U. Time scale is 500 ns per division.

The ORTEC 973U ultra high rate amplifier was an answer for the problem in the previous experiments with Hyperball and Hyperball-2. Figure 7 shows

signals of internal processing (top) and output signal (bottom) of the shaping-amp. The shaping-amp. extracts difference of the signal height with pre-filter which has two humps, *i.e.*, faster reshaping time than that of the ORTEC 671. Resolution of an ordinal semi-gaussian shaping with comparable time scale to the rise time of pre-amp. is worse than that of slow shaping. The pre-filter with two humps, especially the secondary filter, recovers the deterioration in resolution. A pulse height of the fast processing filter is no more relative to energy deposit in a Ge detector but a surface of the output is relative to one. The integrator integrates the signal during 1.5 or 3  $\mu\text{s}$  from the detection of the rising point which corresponds to the start of a  $\gamma$ -ray signal. The energy resolution is 3.3 keV at 1.3 MeV with 3  $\mu\text{s}$  integration. The characteristics of ORTEC 973U are listed in the Table 4. The previous experiments were performed with the 3.0  $\mu\text{s}$  mode.

Table 4: The characteristics of ORTEC 973U ultra high rate amplifier

Gated Integrator [ $\mu\text{s}$ ]	1.5	3.0
FWHM (@1.3 MeV) [keV]	4.7	3.3
Pulse width [ $\mu\text{s}$ ]	1.5	3.0
Reset pulse width [ $\mu\text{s}$ ]	6.0	8.0

### 2.5.2 Problems of the Conventional System

Although ORTEC 973U reduces greatly the processing time, the E13 experiment with a full intensity beam requires more efficient readout method. The dead time of the Ge detectors are caused by the following two reasons:

- (1) Dead time from the processing time of the shaping-amp. and
- (2) Dead time after the reset pulse of the pre-amp., especially an overshoot by the opposite pole input.

In the E13 experiment with the full intensity beam, the solution of the latter becomes more important.

With respect to the first point, the fast shaping with some tricky circuit like the ORTEC 973U is valid. Considering the collection time of the careers in a Ge detector, the processing time of 3  $\mu\text{s}$  is almost the fastest processing

time. The faster processing time than  $3 \mu\text{s}$  may cause the deterioration in the resolution. The dead time occurs during the processing time of the shaping-amp. Figure 8 shows the waveform which causes a pile up at the output of shaping-amps. The top figures are the pre-amp output. At this stage the pile

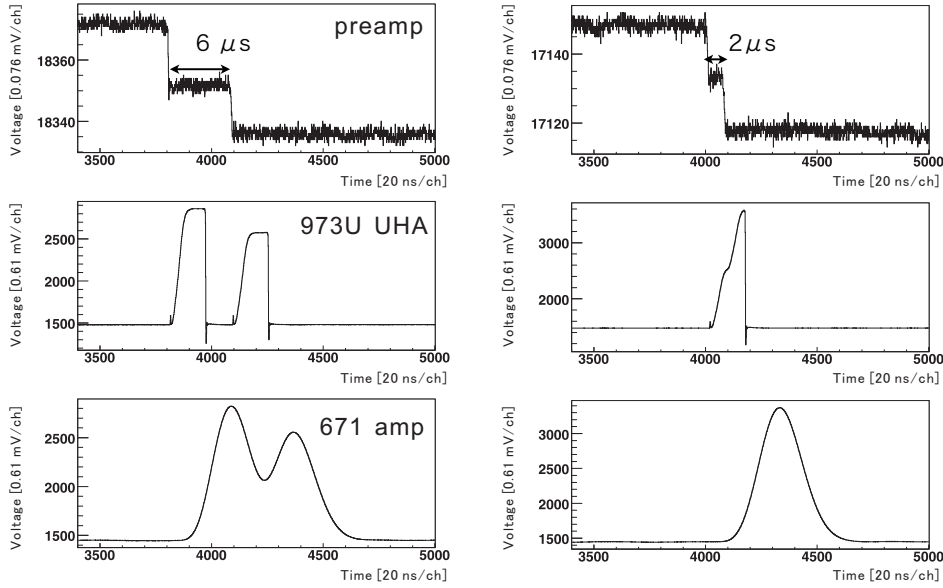


Figure 8: The signals which causes pile up in the shaping-amps section. The top figures are outputs of the pre-amp, the centers are that of the ORTEC 973U ( $3 \mu\text{s}$ ) and the bottoms are that of the ORTEC 671 ( $2 \mu\text{s}$ ). In the left part, only the 671 causes the pile up and both shaping-amps cause the pile up in the right part.

up has not occurred. Intervals of the two signals on the left and the right side are  $6 \mu\text{s}$  and  $2 \mu\text{s}$ , respectively. A pile up signal where more than one  $\gamma$  rays come within a charge collection time ( $\sim 0.4 \mu\text{s}$ ) cannot be separated. The centre figures are the outputs of ORTEC 973U. On the left side, the output of the shaping-amp. does not pile up because the two signals separate each other in  $6 \mu\text{s}$ , which is longer than the gate integration time of  $3 \mu\text{s}$ . On the other hand, the output of the right side piles up as the two signals come within the  $3\text{-}\mu\text{s}$  integration time. The shape of the output signal is distorted

and two signals are not able to separate because the signals are integrated by the capacitor and the second pulse is not charged correctly. The pile up events have to be rejected and contribute to the dead time. The problems for this readout method are that estimation of the full charged height of the first signal and the starting point of the secondary signal are difficult because ORTEC 973U processes input signal with the special filter (the camel filter) and integrates the signal, and the secondary signal is often cut during the integration by the  $3\text{-}\mu\text{s}$  gate time which starts from the detection of the first signal. It is found that the bottlenecks for the more efficient readout are the integration of the signal by a hardware level and the fixed integration time. The problems can be improved by a waveform analysis of the pre-filter. The bottom figures display the output of ORTEC 671. Since the shaping time or the pulse width are much longer than that of the ORTEC 973U as shown in Table 3, both outputs are piled up. Especially the right output looks like already one signal. The ORTEC 671 has a long processing time and pile up event cannot be read correctly by a PHADC which reads the highest position of input signal. The problem is the long shaping time although its output shape is gaussian and can be separated by waveform analysis.

The problems of the conventional system is the use of a PHADC. It is found that for the first point that the waveform analysis has a possibility to reduce the dead time in both shaping-amplifiers.

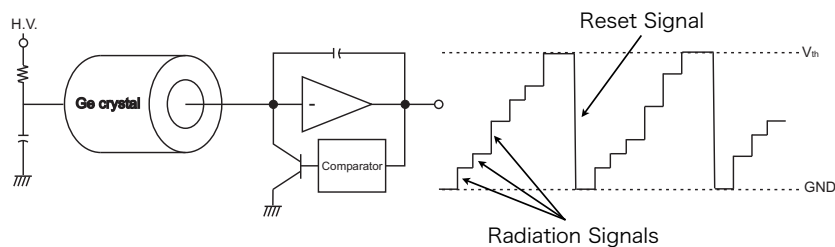


Figure 9: A schematic view of a pre-amplifier. Output signal is also drawn.

With respect to the second point, the dead time is caused by a big ramping of the voltage in a short time interval. A basic structure of a transistor reset type pre-amp. and output signal are drawn schematically in Fig. 9. When a capacitor in the pre-amp. is charged almost full, a sensor detects and

discharges the capacitor. The polarity of the discharge signal is opposite from that of the real one. Although shaping-amps. try to shape the reset pulse, the shaping-amps. are designed not to handle opposite pole, namely, the signal line is clamped by a diode. This is because of the protection of PHADCs which normally accept only one polarity. Indeed, the shaping-amp. processes the reset signal inside the module and takes a long time due to the long input signal of 2 or 4  $\mu$ s. The output after the reset undershoots by the above reasons. The lengths of the undershoot (reset pulse width) are listed in Table 3 (ORTEC 671) and Table 4 (ORTEC 973U).

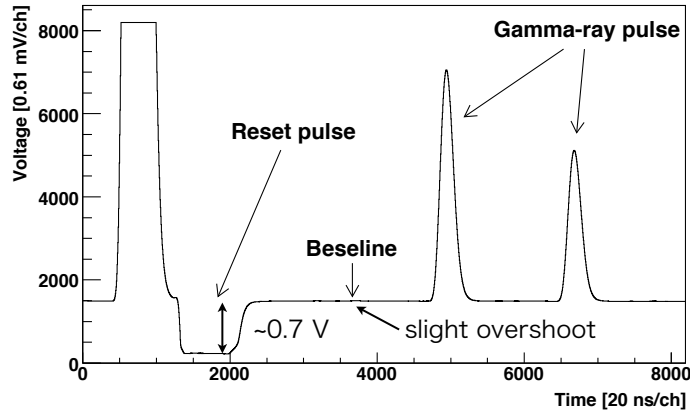


Figure 10: The waveform around the reset (ORTEC 671).

Figure 10 shows the waveform around the reset in case of ORTEC 671. It is found that an output which corresponds to the reset signal is clamped on the diode voltage of  $\sim 0.7$  V ("reset pulse" in Fig. 10). The undershoot region is treated as dead time because radiation signals during the period are not processed correctly. Slightly overshoot follows the undershoot before the base line is restored. This also contributes to a dead time. Thus, the dead time of a few tens micro seconds happens after the reset in case of the ORTEC 973U (over 100  $\mu$ s, ORTEC 671). The waveform readout is also feasible to the problem because the base line shift and signal on the overshoot are possible to be predicted by using the waveform around the  $\gamma$ -ray signal.

The previous experiment had dead time of 30  $\mu$ s after the pre-amp reset with the ORTEC 973U. Total 50 % of dead time occurred with 2 MHz beam

at KEK-PS (Proton Synchrotron). The single rate of the Ge-detector was 50 kHz. It is clear that the full intensity beam (10 MHz) at J-PARC cannot be handled with the ORTEC 973U and entirely new readout system is desired.

## 2.6 Solution to the Problems

A waveform readout method is applicable to the dead time problems. The method records an input signal with a sampling-ADC and analyzes the recorded waveform. The readout method during the pile up and the overshoot was developed by using the sampling-ADC in the previous study. The ORTEC 671 semi-gaussian shaping-amp. was chosen in the study.

With respect to the first problem (1), a pile up signal is separated by using a numerical table function which represents the output signal of ORTEC 671. The reasons that the pile up separation can be performed are as follows:

- The shaping-amp. processes input signals with the Gaussian filter and the principle of the superposition holds for the outputs,
- The shape of the output pulse changes only the pulse height and is independent of the collection time,
- The wave template of a single output of the shaping-amp. can be made and enables the fitting analysis of the pile up signal.

For the second problem (2), the recovery of the resolution have been achieved by the base line fitting. ORTEC 671 has 200- $\mu$ s dead time after the reset. This means about ten times of that of ORTEC 973U. The resolution for a  $\gamma$ -ray peak after 30  $\mu$ s of a reset signal is acceptable by using the waveform analysis method with ORTEC 671. The result means a comparable dead time to ORTEC 973U, and a better resolution (less than 2.9 keV @ 1.3 MeV) has been achieved.

This method analyzes the pulse hight better resolution and less dead time than the direct readout method by a PHADC, but the amount of data is much larger. For example, the minimum amount of data of the waveform which is recorded during 200  $\mu$ s with 100 MHz sampling, 16 bit resolution sampling-ADC is 40 kByte. This is 15000 times the amount of data of the ordinary one word (4 Byte) readout by a PHADC. The large amount of information reduces the transfer speed per event. This means the increase of a dead time of DAQ.

A new readout method which performs the waveform analysis has been designed in order to reduce not only the dead time of shaping-amplifier but also that of DAQ in this study. It is efficient to analyze waveform data on a sampling-ADC module and transfer only data of pulse height for the DAQ problem. The less amount of data transmission enables the less dead time of DAQ. A module which analyzes waveform inside itself is called a digital signal processing (DSP) module. Functions of DSP module are briefly introduced in Section 3.2.

We found that a direct connection of Ge detectors to commercially available DSPs cannot achieve our required resolution of  $\sim 3$  keV (FWHM) at 1 MeV. The dynamic range of DSP is less than that of the reset type pre-amplifier because commercially available DSPs have been designed and used for high gain and resistive feedback pre-amplifiers. Therefore, we decided to insert an interface amplifier (interface-amp.) in front of DSP to solve the problems. The use of the interface-amp. enables that of commercially available DSPs with little modification. The study boiled down to the development of an interface amplifier.

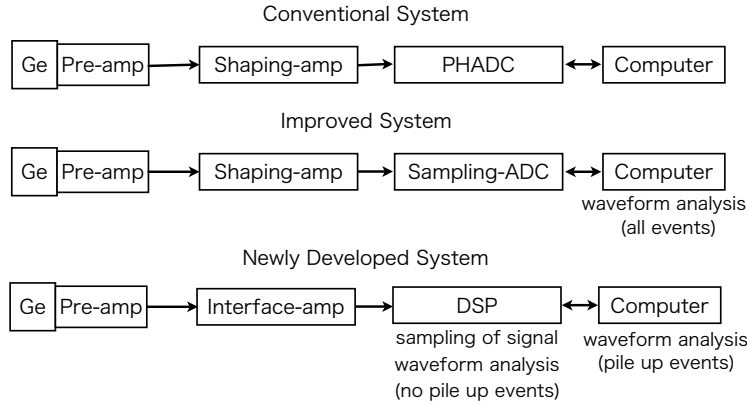


Figure 11: Comparison of the newly developed system with the conventional and the improved (previous waveform analysis) system.

Figure 11 summarizes a schematic view of the conventional system (top), the improved waveform analysis system (center) and the newly developed DSP system (bottom). The conventional readout system acquires only pulse height of the shaping-amp. (ORTEC 973U). The improved system uses OR-

TEC 671 shaping-amp. and samples signal by a sampling-ADC module. All waveforms are analyzed on the computer to get pulse heights. The new DSP system are designed to analyze no pile up event on the module and transfer waveform of pile up event and then analyze the event on computer. The amount of data to be transferred can be reduced by analyzing no pile up event inside the module. The system also has a possibility to solve the overshoot problem after the reset by designing an interface-amp. sophisticatedly.

## 2.7 Philosophy of the Development

The new readout system has been built for the E13 experiment with full intensity (10 MHz) beam. The reduction of the dead time is indispensable in order to handle the high intensity beam environment. Dead times of the readout system are categorized into following two: dead time due to a pre-amp. (charge collection time and reset time) and that due to outside of pre-amp. Since dead time of the pre-amp. cannot be reduced, the reduction has to be achieved by modifying the outside stage.

The new system have been developed with the following concepts:

- The system uses the waveform readout methods,
- The system is built by using as many commercially available parts,
- The product has to need not to be modified as possible,
- The system is designed to be used as long as possible.

The first concept is already discussed in Section 2.5 and 2.6. The system has to be built with a general product in order to use a system for a long term, *i.e.*, the system ought not to be dependent on a particular device. This concept enables the modules in the system to be updated with the growth of the technology. Modifications of a commercially available module have to be minimum because the modifications use much time and have a possibility of causing lots of troubles. Technology of waveform processing and surroundings is remarkably developed for the last decade, especially the sampling-ADC for the high bandwidth and high speed. It is forecasted that the speed of the development will not be slowed down and the use of the waveform readout is not so risky at the present. The last concept is also important. The long term use of a system reduces the total running cost and time for preparation of experiments.

## 2.8 Requirements for the New Readout System

Requirements for the new readout system are described in this section. The requirements consist of three parts of the sampling-ADC, the analog interface amplifier (interface-amp) and the data transfer. These three sections are related to each other. The analog interface-amp is designed considering the properties of a sampling-ADC and a Ge detector.

### 2.8.1 Sampling-ADC

There are several types of sampling analog to digital converter (sampling-ADC) in the world. Sampling ADCs with the 14 bit and 100 MHz sampling are suitable for the purpose of  $\gamma$ -ray spectroscopy. The estimation of the performance is discussed in Section 2.8.2 and 3.1. A few types of ADCs are introduced, and we decide which type is the best for our purpose.

Figure 12 shows a schematic view of input signal and data which is sampled by a sampling-ADC. A resolution of an ADC indicates the number of discrete values over the range of analog values. A  $M$ -bit ADC divides the vertical range of the input signal into  $2^M$  discrete levels. For example, a vertical range of 10 V, the 13-bit ADC, namely, in case of AD413a, digitizes an input signal with a  $10 \text{ V}/2^{13} = 1.24\text{-mV}$  voltage interval. The number of  $M$  and  $N = 2^M$  are called a resolution and a dynamic range of the ADC, respectively. In general high precision conversion takes longer time than the low precision.

In case of a sampling-ADC, it converts an input signal to digital data for the every time interval of  $T$ . For instance, the signal is digitized at the circle points in Fig. 12. In other words, the ADC converts the input signal  $f = 1/T$  times per second. The values of  $T$  and  $f$  are called as a sampling interval and a sampling rate or frequency, respectively. A sampling-ADC whose sampling frequency is  $f$  can record frequency component of input signal up to  $f_n = f/2$ . The value of  $f_n$  is called the Nyquist frequency. Frequency component over  $f_n$  cannot be recorded correctly and is recorded as a fake signal whose frequency is less than  $f_n$  (alias).

It is suitable to use a  $\Delta\Sigma$ -ADC for the slow and high precision conversion like recording of sound. The ADC samples much higher sampling rate (typically over 512 times) than the actual output rate with lower precision and decimates (averages) the data to the desired sampling rate and resolution. This method have a big merit of the easiness in design of an anti-alias filter,

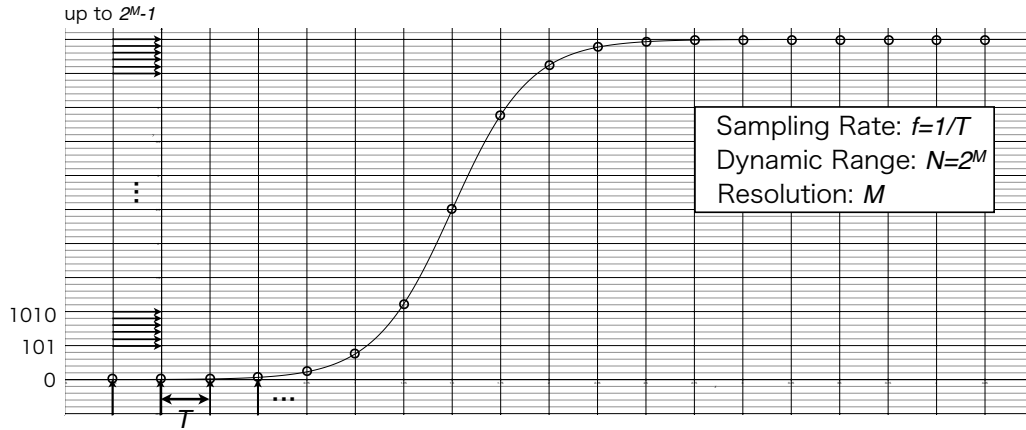


Figure 12: Schematic view of input signal (solid line) and sampled data (circle points) with sampling rate (frequency) of  $f$  and  $M$ -bit resolution.

namely, a low pass filter and reduction of costs. The typical sampling rate of the ADC is from several hundred Hz to 1 MHz and resolution is over 16 bit. For example properties of the ADC for the sound recording are 48 (96) kHz with 16 (24) bit. A flash ADC is used for high speed and moderate precision sampling. A typical resolution of the ADC is 8 ~ 10 bit and sampling rate is over 100 MHz. It is often used for recording of the waveform of scintillation counters with photo multiplier tubes.

The pipe-line ADC is suitable for our purpose. This type is also called flash ADC in the field of nuclear experiment. The resolution and sampling rate are over 10 bit and 10 MHz, respectively. Design of sampling-ADC whose sampling rate and resolution are over 11 bit and 100MHz gets to be more and more difficult and less and less products. The pipe-line ADC with 200 MHz and 14 bit are available in these days. A typical full scale of the ADC is  $\pm 1$  V or 1.5 V. A few products with  $\pm 2$  V input, 100 MHz, 14 bit are also available.

### 2.8.2 The Analog Interface Amplifier

The analog interface-amps have to be designed by considering both properties of sampling-ADCs and Ge detectors (pre-amps.). The amplifier corresponds to shaping-amp like ORTEC 973U in the previous experiment. The most important factor on the designing of the amplifier is to achieve the resolution comparable to ORTEC 973U *i.e.* 3 keV@ 1.3 MeV.

First the connection between an interface-amp. and the sampling-ADC is discussed. As described above, the frequency at which a sampling-ADC can convert the input signal is a half of the sampling frequency which is known as the Nyquist frequency. A signal which has a frequency component higher than the Nyquist frequency is not recorded correctly and recorded like some low frequency signal (alias). Figure 13 shows an example of an alias signal.

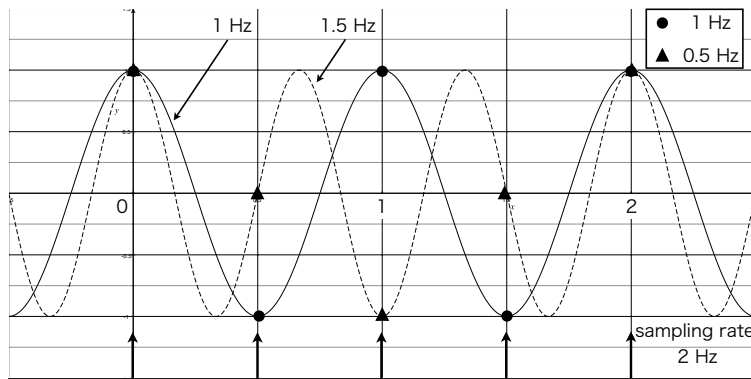


Figure 13: Schematic view of alias signal. A 1.5 Hz sinusoidal signal is recorded like a 0.5 Hz one (triangle points) with 2 Hz sampling. 1 Hz signal is correctly recorded (circle points).

Sinusoidal signals, whose frequency are 1 Hz and 1.5 Hz, are recorded by sampling rate of 2 Hz. Although the 1-Hz signal (the Nyquist frequency, circle) is recorded correctly, the 1.5-Hz signal (triangle) is recorded like 0.5-Hz one, namely, an alias occurs. Since the alias has a false frequency component below the Nyquist frequency, the interface-amps have to be designed to prevent the alias especially in the case of high precision measurement. Forecasting the most high frequency component of the  $\gamma$ -ray signal to be 10 MHz which corresponds to the 100 ns collection time, the lowest sampling rate is roughly predicted to be 20 MHz. The frequency components over 10

MHz have to be eliminated by using the low-pass filter. However, the rapid decimation over the Nyquist frequency affects the lower frequency by a filter character of the "ripple". The ripple of the low-pass filter distorts the input signal and deteriorates the resolution. More moderate low-pass filter has to be designed in order to avoid the distortion of the input signal. Considering the difficulty of the design of the low-pass filter, the numbers of the parts and of course the resolution, the sampling-ADC with the sampling rate over 50 MHz is appropriate and that with 100 MHz is suitable for our purpose.

Second the connection between the Ge detector is discussed. As described in Section 2.5, the main reason for the dead time is the reset signal of the pre-amp. In order to prevent the undershoot and the overshoot, some trick is necessary. The most simple idea is turning off the power of the shaping-amp. The shaping-amp. attempts to shut-down and not to process an input signal in this idea. Actually, the idea does not work well because it takes several hundred micro seconds to turn-off and turn-on the amplifier. Although the direct use of the idea is not realistic, the idea has a opportunity to be used for real experiments with some modification. The essence of the idea is the isolation of an input signal from the processing stage which processes the signal with a long term in the amplifier. Therefore it is enough for the amplifier to isolate the input signal with the power-on state. The modified idea means the signal to be cut and is realized by inserting a switch into the signal line. This idea can reduce an additional dead time after the reset signal.

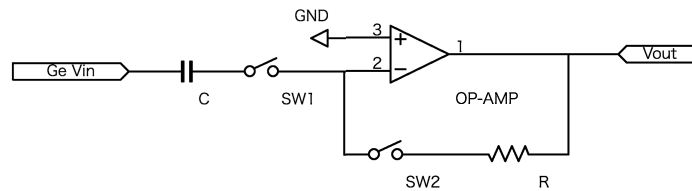


Figure 14: The schematic diagram of the entrance part of a interface-amp. with switches.

Every shaping-amp first extracts the signal step which corresponds to the energy deposit due to the interaction between radiation and the detector.

The function is realized by using a high-pass filter. Figure 14 represents the simplest high-pass filter. The two switches are inserted to cancel the influence of the stray resistance and capacitance in the element of the switch. The switch in the negative feedback (SW2) should be always turned-on, or the output has a possibility of oscillation or an expected action. The switch is made from bipolar transistors (current drive) or FETs (field effect transistor, voltage drive) and commercial products are usually made from CMOS which is a kind of FET in these days. Considering the purpose of the experiment the CMOS switch is a better choice because the signal line from the Ge detector pre-amp. is voltage sensitive and inserting additional current disturbs the circuit. The switch takes several hundred nano seconds to open and close and it takes a few micro seconds to prevent the influences by the change of the gate. Therefore the goal of the dead time is set to be the reset time plus  $2 \mu\text{s}$ . The dead time under the full intensity beam (10 MHz) is comparable to that of the previous experiments (2 MHz) in this condition.

The request for the analog circuit is summarized as follows:

- Inserting low-pass filter ( $f < 15 \text{ MHz}$ ) for the anti-aliasing.
- Flat frequency response, especially from a hundred kHz to several MHz.
- Using switches for the prevention of the undershoot after the reset.

The actual design is carried out by following these requests. The development is divided into two steps; the first is the achievement of the resolution and then the switch is inserted and the whole performance is evaluated.

### 2.8.3 The Data Transfer

In the last several decades, the bottleneck of the data acquisition is data transfer part of DAQ system. Although the DAQ restricts and reduces the performance of the experiments, the condition gets better and better. The propagation of the internet has accelerated the speed of data transfer. We plan to transfer waveform data in the case of only a pile-up event, and transfer one word data during no pile-up event as described in Section 2.6.

The maximum counting rate (single rate) by a Ge detector is predicted up to  $\sim 250$  kHz. Since the amount of data of no pile-up events is one word (32 bit) and it is up to 8 Mbps (1 MBps) in the full intensity beam. Only the no pile-up events transfer, even the moderate speed system like VME (VME-bus IEEE 1014, up to 40 MBps) can handle these event. The problem is transfer of waveforms of pile-up events.

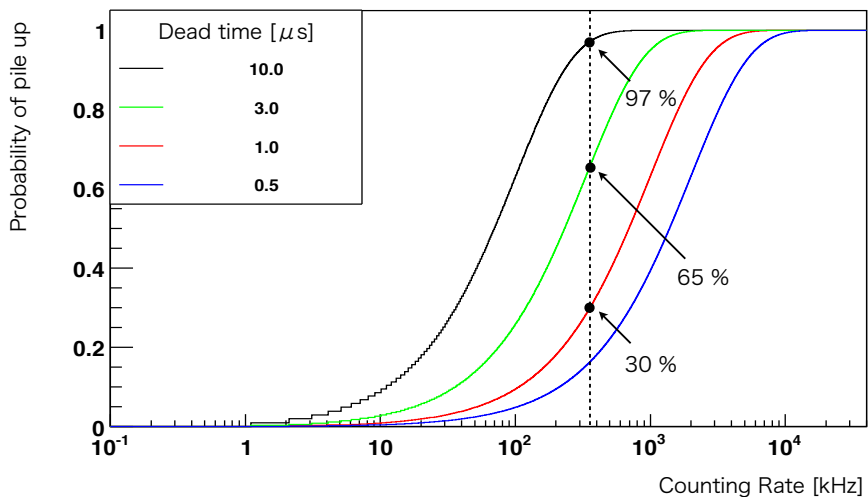


Figure 15: Probability which pile-up occurs with several dead time.

Figure 15 shows probabilities which pile-up event occur in the kHz-order counting rate (single rate) with several dead time. For instance, the 3- $\mu$ s dead time corresponds to that of ORTEC 973U. The probabilities assume that two signals pile up (Fig. 8), for the simplicity. The black vertical line is the maximum counting rate in the case of the full intensity beam at J-PARC. Total 65 % events are piled-up with the 3- $\mu$ s dead time, and the

newly developed system has also  $\sim 3\text{-}\mu\text{s}$  dead time. The amount of data transferred is predicted as follows. A waveform of  $10\text{-}\mu\text{s}$  period around a pile-up event is transferred for the pile-up separation program with a margin. By using  $100\text{MHz}$ ,  $14\text{bit}$  sampling-ADC, the amount of data per event is predicted to  $10\ \mu\text{s}/\text{event} \times 100\ \text{MHz} \times 14\ \text{bit} = 14\ \text{kb}/\text{event}$ . Since total  $250\ \text{kHz} \times 0.65 = 163\text{-kps}$  events are piled-up, the number of events transferred is  $82\ \text{kps}$ . Therefore the amount of data per second is predicted to  $82\ \text{kps} \times 14\ \text{kb}/\text{event} = 1.15\ \text{Gbps}$ . Considering the data size of no pile up event, the amount of data is predicted up to  $1.2\ \text{Gbps}$ .

The value is comparable to the transmission speed of VME 64X *i.e.*  $160\ \text{MBps} = 1.28\ \text{Gbps}$ . This means that total  $32$  VME-bus crates are necessary because a VME 64X crate can only handle a new readout system. The system have to use the ethernet (IEEE 802.3) for the faster and the larger amount of data transfer. The IEEE 802.3-ae supports  $10\ \text{Gbps}$  transfer and hence the data can be transferred to a computer by using the module with the ethernet. All data of Hyperball-J can be transmitted by using the clustered computers. In the case of transferring all data to one computer, data volume becomes  $38.4\ \text{Gbps}$ . The IEEE 802.3 committee is standardizing the  $100\ \text{Gbps}$  transmittal (IEEE 802.3-ba) and it means the data will be transmitted to one computer a few years later.

## 3 The New Readout System

The new readout system is developed according to the development concepts and requirements in the Section 2.7 and 2.8, respectively. The new readout system consists of an interface amplifier and a digital signal processing module (bottom in Fig. 11). In this section, the selection of the readout methods is discussed and then a new waveform processing module called digital signal processing (DSP) module is introduced.

### 3.1 Selection of Readout Methods

Possible candidates for the new system are listed in the following:

- (1) Waveform readout by a sampling-ADC with ORTEC 671 amp.
- (2) Waveform readout by a sampling-ADC with ORTEC 973U amp.
- (3) Direct readout of the pre-amp output by a Digital Signal Processor.
- (4) Differentiation readout of the pre-amp out by a Digital Signal Processor.

With respect to the first two candidates (1) and (2), signal from the each conventional shaping-amplifier is digitized and then the pulse height analysis is performed on a computer (the improved system, center in Fig. 11). With respect to the last two choices (3) and (4), signal from a pre-amp or one from a differentiation amplifier is digitized by a DSP module and the pulse height analysis is performed on the module in case of no pile up and on a computer in case of a pile up (the newly developed system, bottom in Fig. 11) The merits and demerits of these methods are described and compared. Then we judge the best way which is realized by using the up-to-date technology.

#### 3.1.1 Waveform readout by a sampling-ADC with ORTEC 671

The first plan is to record the waveform of the output from the ORTEC 671 shaping-amp. The validity of the waveform readout has been confirmed by using this method in the previous study. In the output signal of ORTEC 671, the only pulse height changes according to the energy and another factors, *e.g.* pulse width or symmetry from the top of the peak do not changes. Therefore the reading the maximum point is enough to make a spectrum. In case of the pile-up, the waveform fitting with the output signal template

separates the signals. The input signals with more than 1  $\mu\text{s}$  interval are separable. No change of the output pulse shape enables the template fitting. The actual waveform slightly changes in the case of pile-up and this phenomena worsen the resolution, but the resolution is still comparable to that of ORTEC 973U. The demerits are that the shaping time is long therefore probability of the pile-up increases and the dead time after the reset is enormous ( $\sim 140 \mu\text{s}$ ). The pile-up signal fitting program at present needs the baseline to be measured otherwise the resolution gets worse than that of the ORTEC 973U. To make matters worse, it is forecasted that the little baseline region is measured in the actual experimental condition. In addition the amount of data increases because of the long pulse width. In the case of 2  $\mu\text{s}$  shaping time, the pulse width is 11  $\mu\text{s}$  (Table 3) and this is almost four times that of the ORTEC 973U (3  $\mu\text{s}$ ).

As regards behavior around the reset,  $\sim 30 \mu\text{s}$  undershoot happens for every reset at present (the reset pulse in Fig. 10). The period of the undershoot is comparable to the dead time of ORTEC 973U without modification. In the case of ORTEC 671 with the switch, it is predicted that the undershoot will be reduced to  $\sim 10 \mu\text{s}$  by considering the slow shaping time of the amp. The dead time is caused by the noise with a  $\sim 2\text{-}\mu\text{s}$  width which appears when the switch opens. Up to a 90- $\mu\text{s}$  waveform after the dead time is handled with the 10 Gbps ethernet (standard at present).

The most important factor to modify the ORTEC 671, a product of AMETEK, Inc., is the cost for the modification. The module is already developed well and there is no space to insert additional parts in the modules. The check of the whole circuit will cost much effort and money. In the case of this methods it is practical to connect a differentiation circuit separately in front of ORTEC 671.

### 3.1.2 Waveform readout by a sampling-ADC with ORTEC 973U

In the case of ORTEC 973U, signal of the pre-filter (top in Fig. 7) can be analyzed by a waveform analysis program in a computer. The signal of the pre-filter is extracted by a bypass of the integrator section. The bypass is performed by a change of a switch on the front panel from the gated integrator pulse (GI) mode to the diode-limited pre-filter pulse (PZ ADJ) mode. The integration of the hump-shape signal is performed in the computer to measure a pulse height, and the integration time can be optimized around 3  $\mu\text{s}$ . The integration program is coded by just summing the waveform during

the integration period. This method can reduce the amount of data less than waveform readout with ORTEC 671 because the shaping time of the pre-filter is much shorter.

Waveform readout with the ORTEC 973U has a difficulty with the pile-up separation because the amplifier processes signal with the special shaping circuit *i.e.* the two humps shaping. As mentioned above, the integral have to be performed on the computer or the pile up separation cannot be handled. This is because the integration stops at 3  $\mu\text{s}$  from the detection of the first signal and the second pulse is often cut (Fig. 8). Coding of the pile-up separation program is a difficult problem. The pulse-heights of the two humps depend on not only the energy deposit in a Ge detector but also the charge collection time of each event. In this case, the waveform fitting with the output signal template does not work correctly. In case of the pile up of the two signal, for instance, total four pulse have to be separated.

Inserting of the switch into ORTEC 973U has a same problem as the case of ORTEC 671. It is predicted that the undershoot of 8  $\mu\text{s}$  will be reduced to  $\sim 4 \mu\text{s}$  and the dead time of  $\sim 20 \mu\text{s}$  to  $\sim 10 \mu\text{s}$ .

### 3.1.3 Direct readout of the pre-amp output by a DSP

This method is the best way for the transistor reset type pre-amplifier if possible. This method is used for most of the commercial digital signal processing (DSP) readout systems of Ge detectors. The pre-amp. output is directly connected to the digital signal processor. The system analyzes the input signal by using the trapezoidal filter realized in a field-programmable gate array (FPGA). The filter works without the pole zero cancellation because the input signal is step function, not like a resistive discharge type. When the reset occurs, the module stops to analyze the input signal with trapezoidal filter. This function is able to be realized immediately by using the logic pulse (TTL) generated from the pre-amp. during the reset period. Furthermore the amount of the output data is comparable to that of a PHADC when no pile up occurs because a field-programmable gate array (FPGA) inside the module analyzes the input signal data. In the case of pile-up, we require the module to output the waveform and the signal should be analyzed by off-line. On the other hand in the case of no pile-up, the module can reduce the total amount of data much less than that of waveform readout methods with conventional shaping-amps described above.

Although the direct readout method is a great idea there are some tech-

nical difficulties in our case at the present (2011). First the resolution of the sampling-ADC is less than the required resolution. As described in the Section 2.3, the Ge detector for Hyperball-J charges carriers up to 150 MeV per reset. On the other hand, the required resolution (FWHM) is 3 keV @1.3 MeV. Considering that a few ADC channels is necessary for 1 keV because the gaussian fitting uses three parameters, the total channel is predicted to be

$$5 \text{ CH} \times \frac{150 \text{ MeV}}{3 \text{ keV}} = 250 \text{ kCH} \quad (4)$$

where it is assumed that five channels correspond to 3 keV. The number of 5 is determined by a case of a peak fitted by the gaussian and a linear background. Considering  $2^{18} = 262144$  and  $2^{17} = 131072$ , it is found that the signal has to be acquired by an ADC with more than 18 bit resolution. However, there are no sampling-ADC with a resolution and a sampling frequency over 18 bit and 50 MHz, respectively. Applying the concept of the  $\Delta\Sigma$ -ADC, we have a plan to use a 200 MHz, 16 bit sampling-ADC as a 50 MHz, 18 bit sampling-ADC. There are a few sampling-ADCs with the required resolution and sampling frequency. They are manufactured by Texas Instruments (ADS5485, USD 98.95 | 1000 chips ) or Analog Devices (AD9467). Since the full range is 2 V, one channel corresponds to 0.03 mV and it is almost the same order as the thermal noise in case of 1 k $\Omega$  termination, 20 MHz bandwidth and 300 K. The thermal noise is calculated by

$$V_{noise} = \sqrt{4K_B \cdot 20 \text{ MHz} \cdot 1 \text{ k}\Omega \cdot 300 \text{ K}} \sim 0.02 \text{ mV} \quad (5)$$

where  $K_B = 1.38 \times 10^{-23}$  J/K is the Boltzmann constant. This relation is known as the Johnson-Nyquist noise. The pre-amp has to be changed to the high power one in order to reduces the input impedance and suppress the thermal noise.

Second is the problem of the dynamic range. The typical range of the ADC is 1 or 2 V<sub>pp</sub>. Device companies begin to put out 3 V sampling-ADCs. The achievement of the good linearity (DL < LSB) makes the sampling-ADC restrained to a low range. <sup>1</sup> The pre-amp. out has to be attenuated into the range in the case of the direct input. The voltage difference for 1.3 MeV is  $\sim 17$  mV for the 2 V full scale. It is also a factor of the deterioration in resolution.

---

<sup>1</sup>DL and LSB are the differential nonlinearity and the least significant bit, respectively.

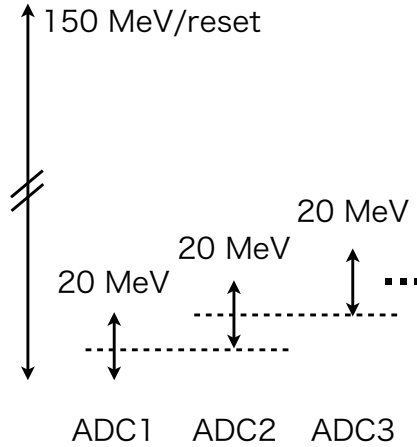


Figure 16: Schematic of the direct readout with several sampling-ADCs.

In order to expand the dynamic range of ADC, we have a plan to use several ADCs to cover the whole range of the pre-amplifier output, as shown in Fig. 16 schematically. However, there are also problems in this method. The idea is shown in the Fig. 16 schematically. A signal from a pre-amp is fed to several sampling-ADCs covering different voltage regions, for example 4 regions, and the sampling-ADCs record the corresponding regions. It is necessary to use more than 4 ( $= 2^2$ ) sampling-ADCs to record the input signal with a required best resolution (18 bit) by using the 16 bit ADCs, or 16 ( $= 2^4$ ) chips by 14 bit ADCs. The system has no margin for 4 chips and one chip acquires 37.5 MeV. The bin width of a channel is 0.6 keV. Considering that the data from the total 32 detectors have to be acquired, the total number of the ADCs is 128. More reliable pattern is described in Fig. 16. A sampling-ADC is required to cover 20 MeV in order to leave a margin because  $\gamma$ -rays from nuclei is up to  $\sim 8$  MeV. In this case, one channel corresponds to 0.3 keV and the signal is enlarged by a factor of 2 (ORTEC) and 5 (CANBERRA). The number of ADCs is 14 for a detector and the total number of ADCs is 448 for performing the experiment. The method has a difficulty in the way of the ground shift with a stability less than 0.03 mV and the way of cutting the region of interest by several sampling-ADCs described in the Fig. 16.

Lastly, as described above (Sec. 2.3), the Ge detectors are exposed to

many charged particles in the experiment. It is different from the normal condition for  $\gamma$ -ray spectroscopy. Almost all of the energy deposit is due to the charged particles. Remembering one pion penetration deposits  $\sim 70$  MeV, a few ADC regions are passed through by one charged particle penetration. For the E13 experiment, the method is not so smart. It is a waste of ADCs and the different system is more efficient for our purpose.

### 3.1.4 Differentiation readout of the pre-amp output by a DSP

This method extracts a difference of a step in the pre-amp output which corresponds to energy deposit in a Ge detector (The differentiated signal in Fig. 5). The module does not acquire the leak current which has different frequency component from the detector. Since charged particle penetration events are not analyzed in our experiment, the full scale is set to 8 MeV, actually 9 MeV with a margin. The dynamic range for the system is predicted to be  $5 \text{ CH} \times 9 \text{ MeV} / 3 \text{ keV} = 15 \text{ kCH}$ , with the same process of Eq. 4. It is enough to use the 14 bit ( $2^{14} = 16384$ ) sampling-ADC, and in the case of a few channel for the 3 keV (FWHM), the system can be handled by the 13 bit one. Furthermore, a channel width of the 14 bit sampling-ADC corresponds to 0.12 mV which is almost six times the thermal noise. The ground level have to be shifted for using the full scale of the 14 bit resolution because bipolar dynamic range is divided into  $2^{14}$  CH, and each polarity has 13 bit resolution. These values mean that the differentiation method is realizable by using technology and market products at present.

The extraction is performed by the high-pass filter *i.e.* differentiation circuit. The requirements for the extraction circuit, especially high frequency components, are discussed in the Section 2.8 as an analog interface-amp. In the low frequency component, frequency components of leak current are estimated as follows: A rest rate is set to 5 Hz as the reset occur once per a few seconds. On the other hand, a conventional shaping-amplifier accepts signal whose decay time constant up to  $100 \mu\text{s}$ , and the corner frequency of the  $100\text{-}\mu\text{s}$  constant is 1.6 kHz. We approximate the output signal of the pre-amp. to the sawtooth wave, and assume all of output signal is due to leak current, although it is over estimation. In this condition, corner frequency is almost 320 times of the reset rate. Contribution of the 320th harmonic to the corner frequency is  $1/320$  ( $-50$  dB). In case of  $50 \mu\text{s}$  (3.2 kHz), the gain is  $1/640$  ( $-56$  dB). The actual frequency component of the leak current is less than 5 Hz, the leak current can be negligible. For the differentiation

circuit, it is enough to consider a relationship between the time constant of differentiation circuit and the acceptable range of pole-zero cancellation.

In summary, by taking account of the development concept, this method is the best way to use the differential readout with the DSP in the four plans. The development of an interface amplifier with a switch circuit is the key of the realization of the fast readout system.

## 3.2 Digital Signal Processing (DSP) Module

In general, it is called digital signal processing (DSP) to process sampled (digitized) waveform data with proper digital filters in real time. The DSP has become widely used with development and spread of the digital architectures in the area of sound, movie, etc. instead of the analog signal processing. Digital signal processing modules mainly consist of A/D part and analyzing (processing) part. The former is realized by the use of sampling-ADC and the latter by the digital signal processor. DSP modules for several radiation detectors have also been developed. In this section, general properties of DSPs for Ge detectors and DSPs for the hypernuclear spectroscopy are introduced.

### 3.2.1 General Properties of the DSP

A conventional system for making a  $\gamma$ -ray energy spectrum consists of a shaping-amp. and an ADC. The ORTEC 973U shaping-amps and ORTEC AD413A PHADCs have been used in the previous hypernuclear spectroscopy experiments. The PHADC whose type is successive-approximation ADC has 13 bit resolution and full scale from 0 to 10 V. The channel width is 1.2 mV and it is ten times that of sampling-ADC with 14 bit and 2 V full scale.

A DSP samples waveforms from the pre-amp and reshapes the sampled data numerically with digital filters. The digital filters are executed on a digital signal processor inside a DSP module in real time. The functions of digital filters are the same as those of shaping-amps. The DSP module extracts information about energy and also timing. The waveform sampling and the digital filtering allow the module to analyze both information. Moreover the real-time processing of waveforms enables the reduction of the amount of data. A DSP for  $\gamma$ -ray spectroscopy mainly contains a field-programmable gate array (FPGA) as a digital signal processor, which is easily applied to the digital filters that are often updated and are dependent on detector types.

The trapezoidal filter is used for the energy analysis in a DSP while the  $CR-(RC)^N$  semi-Gaussian filter is basically installed in conventional amplifiers, even in the ORTEC 973U. Figure 17 shows an example of the semi-

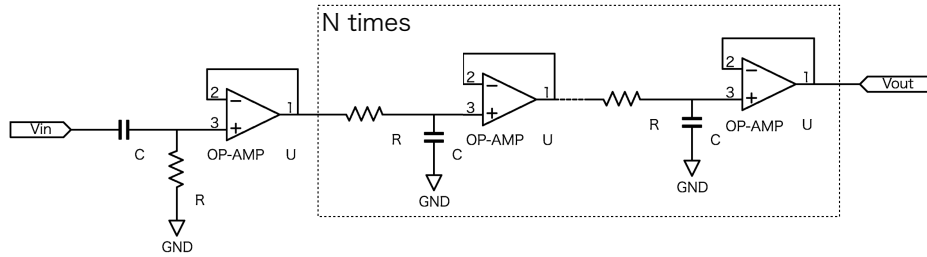


Figure 17: An example of the  $CR-(RC)^N$  semi-gaussian filter.

gaussian filter. The circuit first differentiates an input step signal to extract the difference of the step, and then integrates  $N$  times. Choice of appropriate parts and configuration enables the amplifier to reshape the input signal into a gaussian shape. Figure 18 shows a schematic view of the impulse response of the trapezoidal filter. The dashed line is the input step function and the

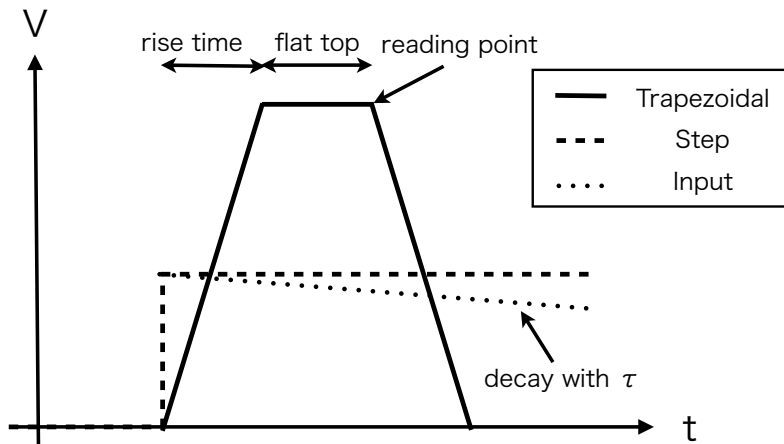


Figure 18: Schematic of a response of the trapezoidal filter (solid line) by a step function (dashed line) and the actual input signal (dotted line).

solid line is the output response of the trapezoidal filter. The actual input signal is also drawn with the dotted line. The rise time corresponds to the shaping time of the semi-Gaussian filter (*e.g.* ORTEC 671). It needs to be set to almost twice the shaping time in order to achieve the energy resolution of the DSP as good as that of the shaping-amp. The flat top is set to recover the deterioration in the energy resolution by the difference of the rise time of input signals. The end point of the flat top is read to make an energy spectrum. The actual input signal which has a decay constant  $\tau$ , typically several tens of microseconds, has to be converted into a waveform without decay because the trapezoidal filter processes only a step function. This function is called pole-zero cancellation (PZC).

Timing detection is performed by leading edge discrimination (LED) or constant fraction discrimination (CFD). These functions are also implemented in digital filters, and are performed in the FPGA. Since the resolution of the timing is less than 1 ns, the DSP has performance for a Ge detector good enough for hypernuclear spectroscopy (FWHM  $\sim 5$  ns or 200 MHz bandwidth). The analyzed timing data is transferred to a computer. On the other hand, the conventional timing detection system consists of a CFD and time-to-digital converter (TDC), and the timing information is also used in a trigger level. DSP module, especially by Techno-AP, has a digital-to-analog converter (DAC) in order to check the operation of several filters. It has a possibility to reduce signal line for the timing detection from the pre-amp. The common use of a signal line for the analysis of energy information and timing detection reduces the troubles by the wiring of signal lines, and reduces noise from outside of the DSP module. However, a DAC with 100-MHz update rate is installed in the module at present. The timing information cannot be used for the trigger level unless the DSP has a DAC with update rate over 400 MHz. Resolution of the DAC is not necessary for this purpose. Fortunately, DACs with update rate over 1 GHz and resolution over 14 bits are manufactured by Texas Instruments (*e.g.* DAC3482, 1.5 GHz, 16 bit) and Analog Devices (*e.g.* AD9779, 1 GHz, 16 bit). We have an opportunity to make a DSP module which outputs timing information for the trigger.

### 3.2.2 DSP Modules

Two DSP modules are almost available for the hypernuclear  $\gamma$ -ray spectroscopy by Ge detectors. One module is manufactured by Techno-AP Co., Ltd. and the other by Lawrence Berkeley National Laboratory (LBNL). The properties of each module are briefly summarized.

#### Techno-AP Module

The APV8008 and APU8004 manufactured by Techno-AP Co., Ltd. (Techno-AP modules) are usable for the reset type Ge detector. The APV8008 is a VME module of 8 channels input type and the APU8004 is a stand alone module of 4 channels type. A VME crate is used just for the power supply. The data are transmitted by the 100BASE-T (up to 100 Mbps) ethernet and transmission protocols are TCP/IP (UDP for the transmission of the larger amount of data per second, an optional extra). For reference, the standards of TCP, IP and UDP are RFC 793, RFC 791 and RFC 768, respectively.

Table 5: The properties of Techno-AP modules

Input Impedance [ $k\Omega$ ]	1
Input Range [V]	$\pm 1$
Resolution [bit]	14
Sampling Rate [MHz]	100
Bandwidth [MHz]	DC $\sim$ 16
Integral Linearity [%]	$\pm 0.0025$
Event Transmission Rate [MBps]	$\sim 1.2$

Table 5 shows characteristics of Techno-AP modules. The input impedance of 1  $k\Omega$  accepts a signal from the pre-amp whose output impedance is low. The modules contain sampling-ADCs which satisfy the system requirements described in Section 2.8. The low-pass filter (up to 16 MHz) is also inserted in front of the sampling-ADC in order to reduce aliasing noise (anti-alias filter). The integral linearity represents that the energy information may shift 0.2 keV for the full scale of 8 MeV. The shifts due to the non-linearity are less than the channel width of the sampling-ADC.

Techno-AP modules accept inputs from both the resistive feedback and the transistor reset pre-amp. The acceptable time constant of the resistive

feedback pre-amp. is over  $40 \mu\text{s}$ . The interface-amp. inside the module (also called pre-amp) reshapes input signal and extracts the difference of the step. Time constants of the interface amplifier are 2.2, 3.9 or  $6.8 \mu\text{s}$ . A value is selected by considering the detector type, rising time of the step, throughput, etc. and the time constant of  $2.2 \mu\text{s}$  is selected for the E13 experiments. The differentiated signal is sampled and then analyzed with the filters. Waveforms

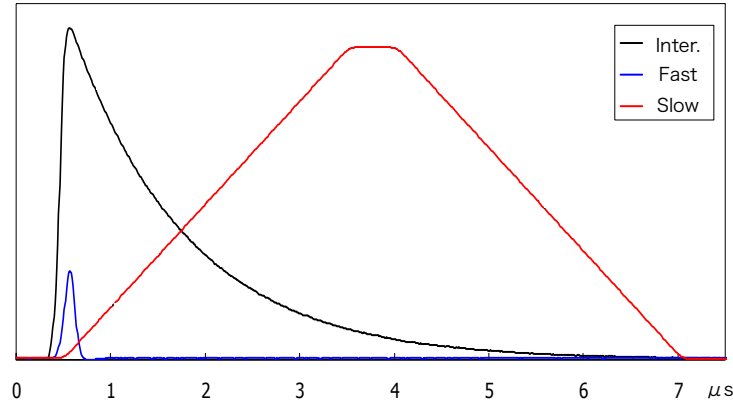


Figure 19: Waveforms in Techno-AP module. The interface amplifier output (black line) is converted to the fast signal (blue line) and the slow signal (red line).

in Techno-AP module are represented in Fig 19. The interface-amp output (black line) is recorded by a sampling-ADC and processed by a fast filter and a slow filter. The fast filter processes waveform of the interface-amp with a faster time constant than that of the slow filter and reshaped the signal (blue line) is used for timing detection and input rate counting. The slow filter converts the input signal to the long-term trapezoidal shape (red line) for making an energy spectrum.

The modules works in multi-channel analyzer (MCA) mode or waveform transmission mode. The modules are controlled by the LabVIEW (National Instruments) software via TCP/IP (UDP). The data are saved in the forms of text files or binary (big endian) files.

The modules are under development. Especially, it was found in this study that the energy resolution was strongly dependent on the prediction of

the base line. There remains issues to have to be revised yet. For example, estimation of counting rate and throughput are not for the use.

### **GRETINA Module**

GRETINA is a new type of  $\gamma$ -ray detector for the study of structures and properties of atomic nuclei and is the first stage of the full Gamma-Ray Energy Tracking Array (GRETA). A DSP module for the GRETINA experiment (GRETINA module) has also being developed.

Specifications of GRETINA module are listed on Table 6. The full scale,

Table 6: Specifications of GRETINA module

Input Range [V]	$\pm 1$
Resolution [bit]	14
Sampling Rate [MHz]	100
Integral Linearity [%]	$\pm 0.1$
Differential Linearity [%]	$\pm 1$
Data Storage Rate [MBps]	$> 10$

sampling rate and resolution are equivalent to properties of the Techno-AP modules. The acceptable signal type for GRETINA module is a differential input in order not to have a sensitivity to noises (mainly from the ground-loop). The value of the integral and differential linearity is less than  $\pm 0.1$  and  $\pm 1$  % over the top 99 % of the dynamic range. The data are transmitted via VME 64X or PCI Express. The transmission rate of the GRETINA module is higher than that of the Techno-AP module at present.

The DSP module accepts only signals from a resistive feedback pre-amp. An interface-amp is necessary in order to use it for the reset type pre-amp. The pick-off board (POB) was designed for as interface-amp at Argonne National Laboratory (ANL). The POB consists of a passive first-order high pass filter and a switch. The switch is installed in parallel with the resistor which is a part of the high pass filter and cut the reset signal.

### 3.3 Present Status of the System

The differentiated readout method with a DSP is selected for the next generational readout system of the hypernuclear  $\gamma$ -ray spectroscopy. Although the DSP modules made a great success of proper resolution with the high gain and resistive feedback pre-amp, the performance has to be measured by using our low gain and reset type pre-amp. Especially the low gain pre-amplifier has a possibility of making energy resolution worse than that of the high gain type.

The development was proceeded in the following two stage:

- (1) Evaluation of the energy resolution by the normal DSP alone and
- (2) Development of the interface-amp for reducing dead time.

The feasibility of using a DSP with our low gain and reset type pre-amp was tested in the first step. Since the energy resolution and its stability are the most important factors for the experiment, the values were measured at several counting rates up to  $\sim 150$  kHz. After confirmation of the validity of using DSP, the interface-amp was designed in the next step.

#### 3.3.1 Test Measurement with Radioactive Sources

The energy resolution and throughput of the system were measured for the first stage. A Techno-AP module (APU8004) was evaluated by using a liquid nitrogen cooled Ge detector manufactured by ORTEC (ORTEC LN<sub>2</sub> Ge).

The experimental setup is schematically drawn in Fig. 20. Signal from

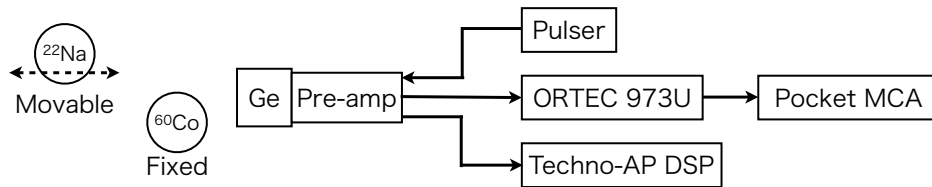


Figure 20: Setup for the evaluation of a Techno-AP module.

the pre-amp was delivered to the Techno-AP module and a reference system. The reference system consisted of an ORTEC 973U shaping-amp whose integration time was  $3 \mu\text{s}$  and a multi-channel analyzer, Pocket-MCA (AMPTEK

Co., Ltd.). The Pocket-MCA has a 13-bit resolution and a 10-V dynamic range. This system is always used as the reference in the Hyperball experiments. The resolution of 1.3 MeV  $\gamma$  ray from the  $^{60}\text{Co}$  source was measured. The  $^{60}\text{Co}$  source was fixed in order for  $\gamma$  rays to hit the detector with a constant count rate ( $\sim 1$  kHz) during the measurement. A pulser (CANBERRA) was used for the estimation of electric noise of the system. The pulse height of the pulser was adjusted to let a peak which corresponds to the pulse in a histogram stand at 1.3 MeV. The  $^{22}\text{Na}$  source was used for the background. The count rate was changed by moving the position of the background  $^{22}\text{Na}$  source from the Ge detector. The reset rates were 4 to 10 Hz during the measurements because the dominant source of the energy deposit was  $\gamma$  rays and charged particles rarely penetrate the detector. Although the condition is different from that of the actual experiments ( $\sim 6.7$  kHz,  $\sim 1$  TeV/s), the behavior of the module around the pile-up can be checked in this condition.

The settings of the DSP were chosen as follows. The rise time and the flat top were set to 1.6  $\mu\text{s}$  and 650 ns, respectively. These values were adjusted by considering of the shaping-time of ORTEC 973U and a fluctuation of charge collection time and by measuring actual resolution. A manner of the parameters estimation is described in Section 3.2. These value achieves performance equivalent to ORTEC 973U about resolution and dead time by pile ups ( $\sim 2.8$   $\mu\text{s}$ ). The dead time of the module is calculated by  $1.25 \times ((\text{rise time}) + (\text{flat top}))$ . The gain was set to  $\times 5$  for our pre-amp. It was also found that the analog gain of  $\times 10$  deteriorated the resolution and could not be used for the experiments.

Figure 21 shows the resolutions versus counting rates (single rate). The top data are resolutions (FWHM) of the 1.3 MeV peak by  $^{60}\text{Co}$  and bottom data are those by the pulser *i.e.* electric noise. The resolutions are obtained by fitting the peak with a Gaussian and a linear background. The pile-up rejector (PUR) was not used in the data set of  $^{60}\text{Co}$  while it was used in those of the pulser. The PUR was used for measuring the influence of the electric noise in case of the pulser. The resolutions of the DSP and the reference are comparable over all of the single rates. The errors which are higher single rates than 100 kCPS are larger than those for less than 60 kCPS because of poor statistics. Electric noise by the DSP makes the resolution worse with increase of the single rate. In the high single rate region, the ground level of the slow trapezoidal filter is shifted by lots of input signals and the prediction of the ground level becomes difficult. The difficulty of precise estimation of the ground level seems to deteriorate the resolutions.

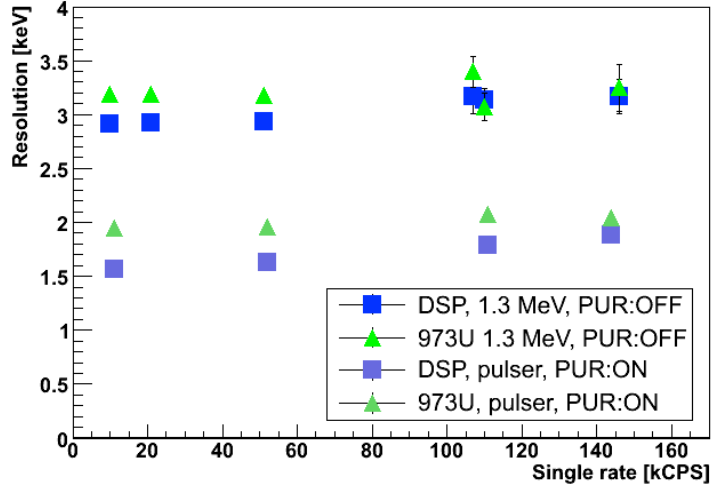


Figure 21: Distribution of resolution versus single rate. Squares are plots of the DSP and triangles are those of the reference system.

Figure 22 shows throughput vs single rate. The throughput is estimated by measuring a peak area corresponding to the signal of the pulser. The peak area is divided by the total number of input pulses by the pulser in a measuring period. The throughput is calibrated by taking into account the DAQ efficiency. The solid line represents a prediction of throughput in the case of  $3\text{-}\mu\text{s}$  dead time, namely, processing time of ORTEC 973U by assuming that only one pile-up occurs. Although the peak area without the DAQ efficiency calibration of DSP is  $\sim 5\%$  better than that of the reference, the throughput of DSP is less than that of the reference as drawn in Fig. 22. This is because of inaccuracy of the count of events inside DSP. The inaccuracy of event counting by the module was discussed in the gamma-ray detector array with energy and position sensitivity (GRAPE) group at Center for Nuclear Study (CNS), University of Tokyo and the bug is being fixed.

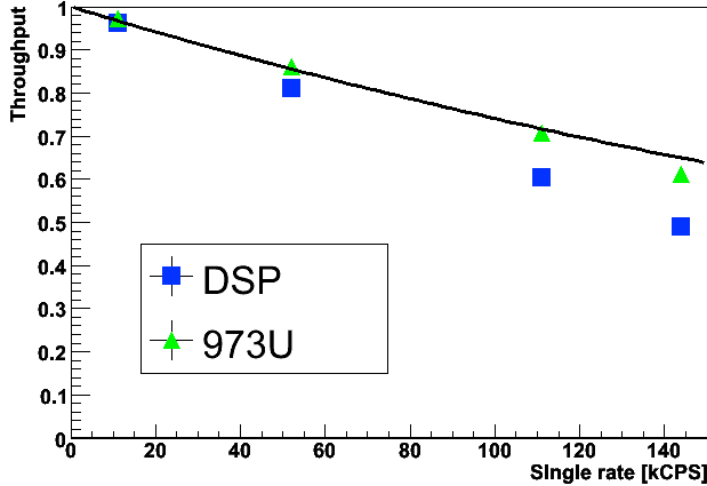


Figure 22: Measured throughputs as a function of the single rate. Squares are plots of the DSP and triangles are those of the reference. Solid line represents a prediction of throughput in the case of 3- $\mu$ s dead time.

### 3.3.2 Points to be Revised

It is found through the measurements that the DSP module has a possibility to be used for the hypernuclear  $\gamma$ -ray spectroscopy with a low gain and reset type Ge detector. However, some modifications are necessary for the actual use in aspects of both the analog part and the digital one.

In the analog part, the module has yet long dead time ( $\sim 100 \mu$ s) after the reset with the slow filter. Although a developer of Techno-AP module modified a firmware to veto the reset period, the dead time of  $\sim 30 \mu$ s remains yet. Development of an interface-amp with switches for fast restarting of measurement is indispensable.

Furthermore, it is found that intermediate frequency noises from a few tens kHz to several hundreds kHz worsen the resolution in DSP. This is because of conflicts between the frequency component of the electric noise from the power supply of the mechanical cooler for the Ge detector and the frequency character of the interface-amp. The interface-amp. needs wide frequency band in order to achieve a good resolution, but the frequency band includes the frequency components of the noises. Analog shaping-amps.

use integral circuit for the reduction of the noise component. Figure 23 shows filtering areas of both DSP and ORTEC 973U. Although DSP basically

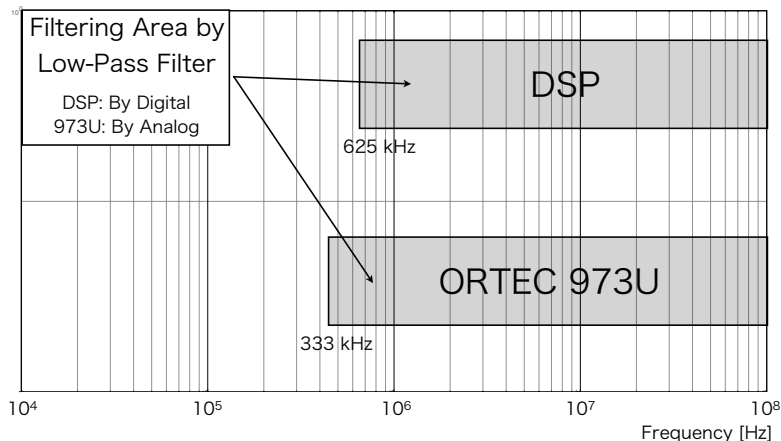


Figure 23: Schematic view of filtering area. ORTEC 973U filters wider area than DSP.

integrates (actually sums) the  $1.6\text{-}\mu\text{s}$  period by the trapezoidal filter, ORTEC 973U integrates the  $3\text{ }\mu\text{s}$  by the capacitor. It is found that the longer shaping time can filter the lower frequency area. While the interface-amp. for the DSP cannot contain the integral circuit because the module performs faster shaping than conventional shaping-amps and for the timing detection. Plans for the noises are development of the frequency filter or the re-purchase of a cleaner power supply. The frequency filter will be realized by the fast fourier transform (FFT) and the noise filter. The key of the development is real-time FFT program which has to be performed twice in a cycle of FPGA. The re-purchase of the power supply solves the problem fundamentally but it costs to purchase power supplies again.

The differential signal transmission is generally stronger against ground-loop noises than the ground-to-signal transmission. The former methods is more suitable for the low gain and reset type Ge detector. The GRETINA module has an advantage in this aspect.

In the digital part, it is found that the prediction of the ground shift in the analysis program is a key to achieve a good resolution. The low gain detector is more sensitive to the predicted ground level than the high gain

one. Actually, the resolution has been improved from several keV to 3 keV @ 1.3 MeV in the previous measurement (Section 3.3.1). The improvement is due to the update of the digital filter, especially the estimation method of the ground shift. Since the prediction methods is dependent on the filter type, the program of the ground level prediction has to be coded for the new interface circuit.

Techno-AP modules support waveform transmission mode and MCA. The waveform transmission mode outputs waveform from the interface-amp (pre-amp out in the manual), slow and fast filters. In the case of pile-up, the two signals have a possibility to be separated by the off-line analysis. The MCA mode analyzes recorded waveform by the slow filter and makes a histogram. Since the histogram data is transferred to a computer, the MCA mode reduces data size. The combination of the MCA mode and the waveform transmission mode is suitable for the hypernuclear spectroscopy, *i.e.* the energy (pulse height of the slow filter) and the time stamp of each event are normally enough and the waveform of the interface-amp has to be transferred in the case of pile-up. The switch of the transmission mode is realizable by using the function of the PUR which monitors whether a pile up occurs or not and is already coded. The histograms of the MCA mode and the off-line analysis can be combined with monitoring the  $\gamma$ -rays for the system calibration.

The actual problem of the development is that the readout methods of Techno-AP modules are hidden as a company secret. The users cannot watch what the module processes. The modules have yet some bugs about the count rate monitor, the data transmission, etc. While the GRETINA module is made by the national laboratory in U.S. and the users are allowed to watch and modify what the module handles on the FPGA. This is great advantage of the GRETINA module. However, it is designed for the high gain and resistive feedback pre-amp and hence some modifications are also necessary in the software part. <sup>2</sup>

---

<sup>2</sup>Unfortunately, the earthquake on 11 March 2011 forced the development of Techno-AP modules to quit. The GRETINA module is the only one module which can be modified for the hypernuclear spectroscopy at present. The development of interface-amp for the GRETINA module has become more important.

## 4 Design of the Interface Amplifier

Interface amplifiers are designed by following the general concept (Section 2.7) and the requirements (Section 2.8). Taking into account the above discussion about the DSP (Section 3.3.2), a first order high pass filters and a second order high pass filter are designed. The formers are designed for GRETINA module and the latter is for both modules.

### 4.1 Factors for Achievement of the Requirements

The resolution of 3 keV @ 1.3 MeV is the most important requirement for the experiment. The interface-amp which worsen the resolution cannot be used. The key point for the achievement of the resolution is how to insert a switch into circuits. Fortunately, Techno-AP modules achieved the resolution requirement. It is therefore noticed that the switch has to be inserted into a line which does not disturb the main signal line of the interface circuit.

The main sections of the interface-amp need to have a flat frequency response. The flat response enables the faithful transmission of input signals. While a switch has distorted frequency response and it deteriorates the resolution. The recovery from the distorted frequency response depends on not only production type but also individual variability of switches and it is not so practical to remove such a difference. Therefore the original plan in Fig. 14 in which the switches are inserted in series with the main line is not used for the above reasons.

The solutions may be the following two methods:

- (1) Inserting switches in parallel with the main line.
- (2) Using a switch to short the circuit.

A switch should be turned off during the true signals or radiation signals being input and vice versa. Both methods are based on the idea that the high off-state resistance does not disturb the main line and the on-state distorted frequency response is not an issue in the case of the reset signal. The interface-amps are designed according to the ideas.

Figure 24 shows a schematic diagram of a differentiation section and a switch section of both the original idea (Top) and the improved methods (Bottom). In the case of the original circuit, the frequency property of the switch affects the signal line, and a deterioration of the resolution is predicted.

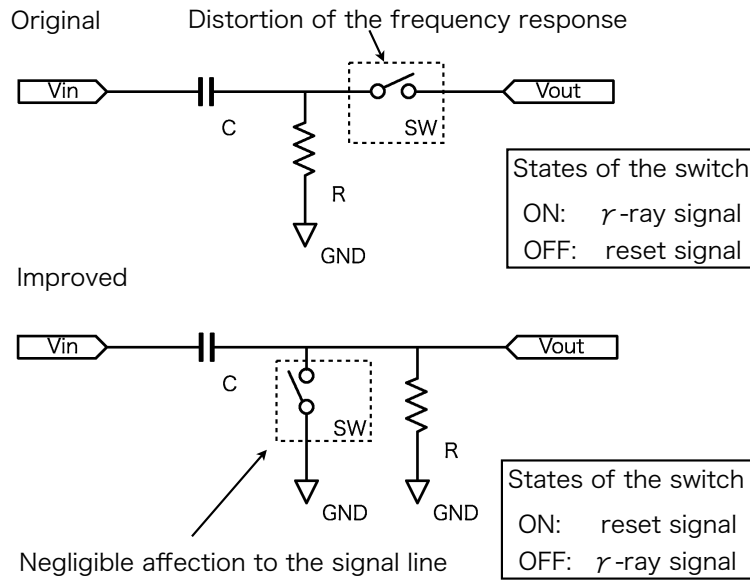


Figure 24: Schematic view of the original method and the improved method of the switch insertion.

Therefore the fast reset recovery circuit is modified into the bottom diagram. The improved circuit satisfies above requirements (1) and (2). A low on-state resistance works as a protection resistance and enables fast recovery after the reset. Influences to the signal line due to the insertion of the switch is negligible in this alignment by the above reasons. It is found that the improved circuit is achievable the required resolution.

CMOS switches manufactured by Texas Instruments (TI) have high off-state resistance and flat response. Switches by TI have flatter property than ones by Analog Devices (AD). Although the interface-amps. are designed not to be influenced by the flatness of frequency response of the switch, the flatness of the on-state is still important for fast discharge of the capacitor. The switches by the TI are chosen in the development.

## 4.2 ANL Pick Off Board

The pick off board (POB) is designed for the interface amplifier of GRETINA module at ANL. The POB enables GRETINA module to be used with the transistor reset type pre-amp. The POB contains amplifiers for the input from a Ge detector, PWO background (Compton) suppression counters, etc. The main line for the Ge detector is used for the E13 experiments. The POB accepts only positive input because pre-amps for Ge detectors at ANL are positive output type.

The main line, or signal line for a Ge detector, of the POB is shown in Fig. 25. The functions are divided into five sections of an input buffer, a differentiation circuit (A in Fig. 25), a reset detection system and switches (B and C), a buffer which separates the differentiation circuit part and output section (D) and differential output amplifier. The sections from (A) to (D) are important for the development. Each section is briefly introduced.

First, the input buffer accepts signal from the pre-amp. with high impedance inside the OP-amp. An AD847 (AD) is used for the buffer. The bandwidths and the slew rate at  $\pm 15$  V supply are 12.7 MHz and  $300$  V/ $\mu$ s, respectively. The slew rate ensures the faithful transmission of an input signal (from  $\sim 25$  mV/ $\mu$ s to  $\sim 3$  V/ $\mu$ s). The gain is set to be unity and can be changed to a higher gain.

Second, the differentiation circuit (A) extracts difference of the signal. The time constant is  $RC = 1$  k $\Omega \times 0.033$   $\mu$ F = 33  $\mu$ s. The frequency components less than the corner frequency (= 4.8 kHz) are cut with  $-20$  dB/dec. The differentiation circuit has no ripple in the frequency domain over the corner frequency because it consists of the first-order filter. This property is suitable for the high precision data acquisition.

Third, the reset detection system (B) detects the reset pulse automatically. It consists of a comparator (LM311, TI)<sup>3</sup> and a flipflop (74ALS74, TI) with a resistive feedback timer. The threshold level can be set from 0 V to -120 mV by a variable resistor. In this circuit, polarity of the reset pulse is assumed to be negative. Time transition of the reset system is briefly drawn in Fig. 26. When a reset occurs and the reset signal becomes lower than the threshold level, the LM311 outputs positive voltage. The output voltage is clamped to 5 V which is the true-stage voltage of the TTL logic. The flipflop sets the output Q connected to the switch onto high-stage and

---

<sup>3</sup>A LM311 was originally produced by National Semiconductor (NS). NS has been acquired by TI on 23rd Sep. 2011.

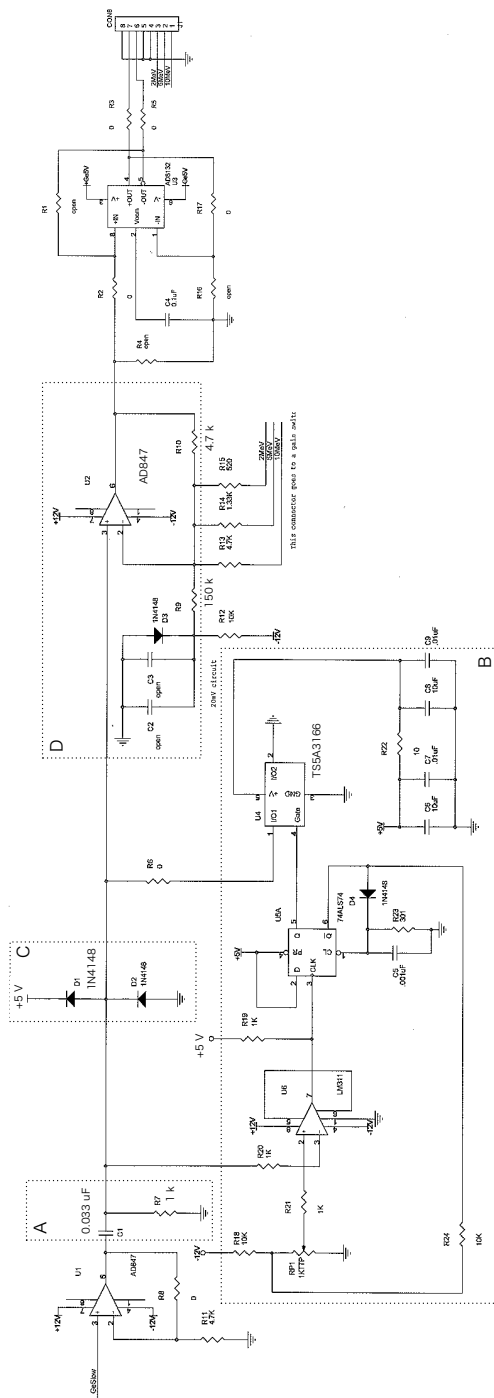


Figure 25: Schematic of POB.

the other side  $\overline{Q}$  on low-stage until the timer reverses the on-off state. The timer which consists of resistance (R23) and capacitance (C5) is connected to  $\overline{CLR}$ . After the voltage of the timer crosses the low-stage level (0.8 V), the  $\overline{CLR}$  resets the on-off stage. The length of the timer can be changed by the values of the resistance and capacitance, and the gate is opened during 30  $\mu\text{s}$  by the actual measurement.

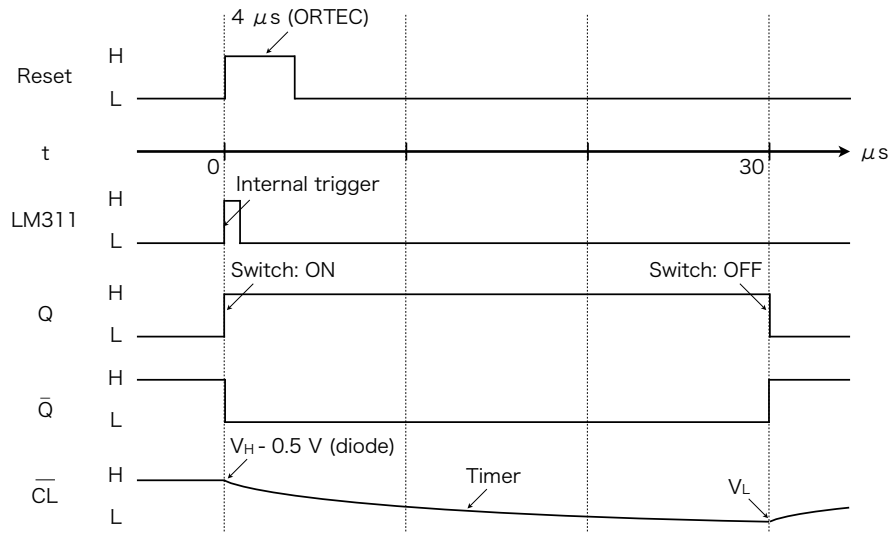


Figure 26: Time transition of the reset logics.

The switch shorts the differentiation circuit (A) with an internal resistor of  $0.9 \Omega$  while the Q is set to high. The TS5A3166 single-pole single-throw (SPST) switch is used. A bandwidth of the switch is 200 MHz and almost flat (within  $-0.5 \text{ dB}$ ) up to 20 MHz. The protection diodes (C) are inserted so that the voltage of the signal line does not exceed the voltage range ( $-0.5 \text{ V} \sim 5.5 \text{ V}$ ) of the switch. Diodes which are used in the POB are 1N4148 whose forward voltage of the diode is 0.5 V at  $25 \text{ }^\circ\text{C}$ . This means the signal does not exceed the rated voltage.

Fourth, the buffer (D) separates the differentiation circuit part (A) and the output part. The AD847 is used for the buffer and configures a non-inverting amplifier circuit. The gain of the buffer is calculated to be 1.03. The gain is able to be changed by altering the value of the resistance. The buffer has also a ground level shifter. The voltage of the cathode side of the

diode is  $-0.5$  V and then the buffer outputs  $+17$  mV.

Lastly, a differential output amplifier is installed. This is for the readout mechanism of the sampling-ADC in GRETINA module. An AD8132 (AD) is chosen, and the bandwidth and slew rate are 350 MHz and  $1200\text{V}/\mu\text{s}$ , respectively. The gain is set at 2. The capacitor of  $0.1 \mu\text{F}$  is inserted in the  $V_{\text{com}}$ -pin for the improvement of the power supply rejection ratio (PSRR). The PSRR describes the amount of noise from a power supply, which the amplifier can reject.

POB does not have a low-pass filter for the anti-alias filter but two AD847s slightly reduces the high frequency component. The gain at 50 MHz is reduced to  $\sim -20$  dB ( $\times 0.1$ ) at the output of the buffer (D). Since POB is designed for the high-gain pre-amplifier and the polarity of some of our Ge detectors are positive and the others are negative, some modifications are necessary for the Ge detectors used for Hyperball-J.

The behavior of POB around the reset signal was measured at ANL and POB was confirmed to work. The dead time is now set to be  $30 \mu\text{s}$ . The value can be reduced to 1.5 times of the reset pulse. This means the dead time of Ge detectors at Tohoku univ. are able to reduce to minimum of  $3 \mu\text{s}$  (CANBERRA) and  $5 \mu\text{s}$  (ORTEC). In the case of actually use in the short reset time, some modification is also necessary in the comparator section in order for the comparator to have more hysteresis. Furthermore the decay time constant of POB is  $33 \mu\text{s}$  as described above. The value is shorter than the acceptable range of pole-zero cancellation feedback of the conventional shaping-amps (more than  $40 \mu\text{s}$ ). The time constant has to be set longer in order to achieve a good energy resolution with POB.

### 4.3 The interface amplifier for the Tohoku Ge-detector

Two interface-amps optimized for our Ge detectors were designed. One is an amplifier for the Techno-AP module and the other is for the GRETINA DSP module. The former has a comparable time constant to the amplifier in the Techno-AP module. The latter is an improved version of POB and the decay time constant is adjusted for the conventional shaping-amps. These amps. are made from well spreading products. The former consists of a second order differentiation filter, and the latter of a first order circuit.

A second order high-pass filter with switches is newly designed. The filter rejects lower frequency components with  $-40$  dB/dec than the corner frequency. Ge detectors for the E13 experiment have low frequency noises due to mechanical vibration by the pulse tube refrigerator. A design of a higher order filter is effective to reduce the influence of the noise. On the other hand, all of higher order filters are made from the combination of a first order filter and a second order filter. It is found that a design of a second order filter with fast recovery time is enough because the first order circuit is already designed.

#### 4.3.1 The Interface Amplifier for Techno-AP Module

The new interface-amp. for the Techno-AP module is designed with a second order high-pass filter and switches. Figure 27 shows the schematic diagram of the circuit configuration. The amplifier consists of three stages *i.e.* a buffer for accepting input signals, a second order high-pass filter and a gain adjustment buffer. In this step, the differential output buffer does not have to be installed because the check of behavior around the reset is main task, and the output signal is checked by an oscilloscope which samples the normal (unbalanced) input signal.

First, function of the buffers is the same as that of POB. LF356 (TI) OP-amps whose bandwidth and slew rate are 5 MHz and 20 V/ $\mu$ s are used, and these specifications are enough for our Ge detectors. The narrow bandwidth is used for the anti-alias filter. The gain at 50 MHz is expected to be from  $-15$  dB to  $-20$  dB by characteristic of the open-loop gain. The total gain at 50 MHz is predicted to be  $\sim -60$  dB since total three OP-amps are used in series. Gains of the input buffer are adjusted by the variable resistors and these are set to  $\times 2$  (CANBERRA Ge detector) and  $\times 1$  (ORTEC Ge detector). The input impedance for the positive input (CANBERRA Ge

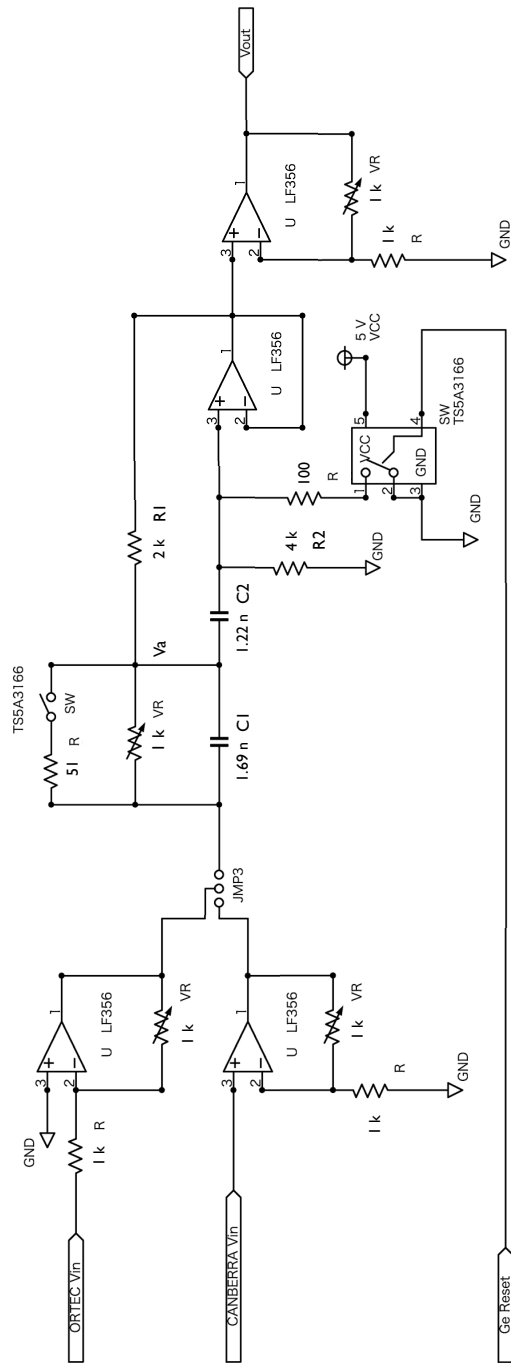


Figure 27: Circuit diagram of the interface-amp for Techno-AP.

detector) is that of the LF356 ( $10^{12} \Omega$ ). It can be reduced by inserting resistance (normally  $1 \text{ k}\Omega$  for the Ge detector) between the signal line and the ground. On the other hand the input of the negative side (ORTEC Ge detector) is terminated with  $1 \text{ k}\Omega$  resistance. A jumper is used to chose the corresponding circuit according to the input types in order not to disturb frequency components of the input signal.

Second, the high pass filter is realized by a Sallen-Key architecture. Reasons for the choice of the Sallen-Key architecture are as follows: the high-pass filter is designed with unity gain; the number of parts is less than multi-feed back circuit, namely, the filter has a simple architecture and it is easy to make and insert the switch. First, a main characteristic part of the high-pass filter without any additional functions is designed and then options (a pole-zero cancellation circuit and switch circuits) are inserted.

Achievement of the good resolution is achievable by the flatness of the filter and the good step response *i.e.* little overshoots and ringing. A Bessel-filter satisfies the requirements. The values of the resistors and capacitors ( $R1 = 2 \text{ k}\Omega$ ,  $C1 = 1.69 \text{ nF}$  pair and  $R2 = 4 \text{ k}\Omega$ ,  $C2 = 1.22 \text{ nF}$  pair) are chosen in order for the filter to have a character of the Bessel-filter. The cut off frequency is  $98 \text{ kHz}$ . The property is slightly different from that of the Bessel-filter because of values of available devices. In this step, namely, only to check behavior around the reset signal, E16 (20 % error, JIS C 5063 in Japan, IEC 63 for international) elements are used. For the manufacture step, the use of elements over E24 (5 % error) are strongly recommended.

An pole-zero cancelation circuit is needed in order to cancel undershoot of the processed signal. It is inserted in parallel with the capacitor of the first differentiation circuit ( $C1$ ) in this design. A variable resistor is used for the adjustment and the value of  $1 \text{ k}\Omega$  is set by default. As can be seen immediately, DC component of the input signal is divided by the resistance of both the pole-zero cancellation feedback  $VR (= 1 \text{ k}\Omega)$  and one of  $R1 (= 2 \text{ k}\Omega)$ . The DC component recovers undershoot of the second differentiation circuit ( $C2 \cdot R2$ ).

Switches are installed to shorten the undershoot by the reset signal. For the first differentiation circuit ( $C1 \cdot R1$ ), the closed circuit which consists of a switch (TS5A3166, TI),  $51 \Omega$  resistor to reduce inrush currents and the capacitor ( $C1$ ) processes the reset signal with a small time constant  $VR \cdot C1 = 51 \Omega \times 1.69 \text{ nF} = 86 \text{ ns}$ . For the second differential, the  $100 \Omega$  resistor and the second capacitor processes with  $120 \text{ ns}$ . The influences of these switches are negligible during the off-stage because off-stage leakage

current is very small (typ. 4 nA and max. 20 nA). The switching is operated by the reset logic signal (TTL) from a Ge detector with 50  $\Omega$  termination. The first switch restricts amplitude of the input signal up to 5.5 V which is the absolute maximum rating voltage of the switch.

Third, a gain of the gain adjustment buffer is variable by a resistance feedback. The buffer is a non-inverting amplifier. The gain is set to  $\times 1$  in the case of ORTEC Ge detector.

Behavior around the reset is simulated and it is confirmed that the output signal is stabilized within additional 2  $\mu s$  *i.e.* the total dead times are 4  $\mu s$  (CANBERRA) and 6  $\mu s$  (ORTEC), respectively. Actually the switching time ( $< 1 \mu s$ ) is added. The bandwidth of the finally designed filter becomes narrower than that of the original Sallen-Key configuration but no ripple occurs and the main frequency region of the Ge detector is not influenced by the pole-zero cancellation feedback.

### 4.3.2 The Interface Amplifier for GRETINA Module

The interface amplifier for GRETINA module (Tohoku-POB) is designed by modifying the original POB (ANL-POB). The concept is the same as ANL-POB. Tohoku-POB is also designed for operation with the shaping-amp. (ORTEC 973U) in order to reduce dead time of the present system. Figure 28 shows a schematic diagram of Tohoku-POB. The figure shows only a negative input part but a positive input part is also implemented. The positive buffer is drawn in Fig. 27. Total two OP-amps are used in series for the signal line and hence the total gain at 50 MHz is predicted to be  $\sim -40$  dB. The Tohoku-POB implements a newly designed full-automated switch, on a trial basis.

Tohoku-POB consists of an input buffer, a first-order high-pass filter with the newly designed switch and a gain buffer. The differential output (Fig. 25) has to be implemented for the actually use with a GRETINA module. ORTEC 973U also accepts the differential input, the implementation of the differential output is strongly recommended. Since functions of the input buffer and the gain buffer are already introduced above, only the improved sections *i.e.* the high-pass filter and the automatic switch section are discussed here.

The time constant of the differential circuit is set to  $RC = 5.1 \text{ k}\Omega \times 0.01 \text{ }\mu\text{F} = 51 \text{ }\mu\text{s}$  because the shaping-amps accepts signals with more than  $40 \text{ }\mu\text{s}$  time constant. The cut-off frequency is  $(2\pi RC)^{-1} = 3.1 \text{ kHz}$  in this condition. No pole-zero cancellation feedback is installed because input signal is a step function.

The automatic switch is developed by improving the original working principle of the switch system in ANL-POB (block B in Fig. 25). ANL-POB detects the reset signal by monitoring negative input with the comparator and the switch is turned on after the detection. Since the switch can accept signal from  $-0.5$  to  $5.5 \text{ V}$ , the diode clamps (block C in Fig. 25) are installed for the protection of the circuit. In the case of the step function, there are no undershoot after the differentiation circuit ( $RC$ ), and the reset signal is grounded by the switch. The protection diode for the negative polarity is just installed in the case of setting an improper threshold voltage by mistake. The diode is not needed if users make no mistake. A module which forces users not to make a mistake in a hardware level is safer than one in a manual book level. Considering the true signal does not across the ground level, function of the switch is summarized to short negative signals. It means that an ideal diode performs the function by connecting it between the ground

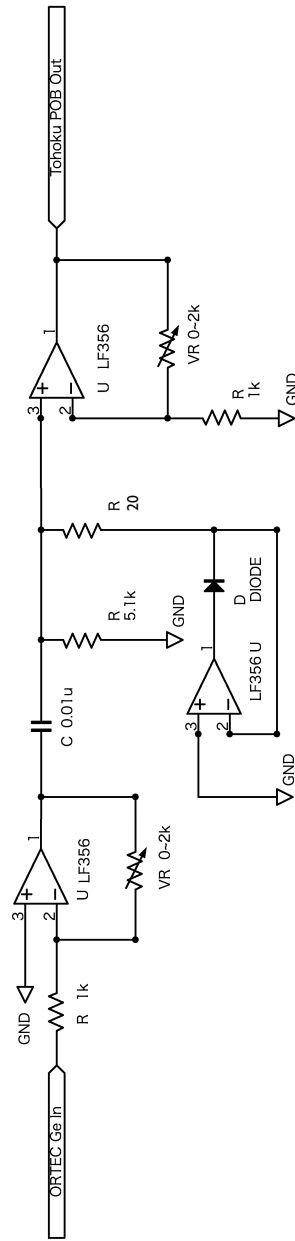


Figure 28: Schematic diagram of Tohoku-POB for ORTEC Ge detector.

line (anode side) and the signal line (cathode side).

The problem is how to make an ideal diode from commercial products in the market. Fortunately the quasi-ideal diode is composed by inserting a market diode into a feedback circuit of an OP-amp. The LF356 and a normal diode whose threshold voltage is 0.7 V are chosen for the moment. In these conditions, the inrush current is expected to appear due to the narrow bandwidth of the OP-amp and the high threshold voltage when the diode switch is turned on. The protective resistance of 20  $\Omega$  is inserted in series to the diode switch and the value of the resistance can be reduced by using a wide bandwidth OP-amp and a low threshold diode. A resistance whose value is equal to or less than 20  $\Omega$  appears an overshoot after the reset signal by a circuit simulation with a 10 MHz OP-amp. In the case of 20  $\Omega$ , the overshoot is small ( $\sim 15$  mV), and it is acceptable with DSP because DSP analyzes not only signal but also ground shift.

ANL-POB is finally modified to the circuit in Fig. 28. The stability of the circuit is ensured by connecting the positive input of the OP-amp on the ground. The maximum voltage limit of the differentiation circuit ( $CR$ ) can be raised from +5.5 V to the power supply voltage of OP-amps (+12 V) by removing the SPST switch (TS5A3166). In the case of the use of conventional shaping-amps, this means the total gain is increased to 2 (ORTEC) and 4 (CANBERRA) with the severe condition of an infinite decay time constant or the step function. On the other hand, the total gain can not be set to so large because the maximum voltage is still +1 V in the case of GRETINA module. Fortunately, the problem can be solved by shorten a time constant of the differentiation circuit.

## 4.4 The Operation Check

Behavior of the newly designed circuit around the reset signal was examined with an oscilloscope. The setup of the operation check is drawn in Fig. 29. The energy signal was input to an interface-amp. The reset logic signal was

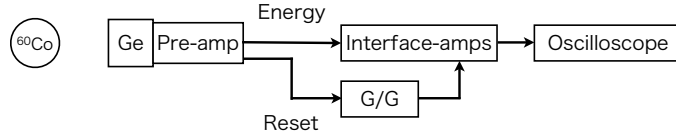


Figure 29: Setup of the interface-amp operation check.

firstly input to a gate and delay generator (G/G) and then connected to the amplifier. The time width of the reset logic signal is changed by using the gate and delay generator for finding a suitable width of the inhibition. Firstly, the width were set from  $2\ \mu\text{s}$  (CANBERRA Ge detector) and  $4\ \mu\text{s}$  (ORTEC Ge detector) to  $4\ \mu\text{s}$  and  $6\ \mu\text{s}$ , respectively. These additional  $2\text{-}\mu\text{s}$  dead time were stabilization time of the switch circuit as described in Section 2.8.2. An ORTEC Ge ( $\text{LN}_2$  cooling) was used for the check because the rump (reset) voltage is higher than CANBERRA one. Problems found in this check are fed-back to the improved version.

### 4.4.1 The Interface Amplifier for Techno-AP Module

A picture of the home made interface-amp. is shown in Fig. 30. The amplifier accepts both positive and negative inputs through a BNC <sup>4</sup> cable and a reset logic signal through a LEMO <sup>5</sup> cable and electric power via D-sub 9-pin connector. The amplifier also outputs signal from the opposite side through a LEMO cable.

Output signals of the interface-amp. for 1.17-MeV and 1.33-MeV  $\gamma$  rays from  $^{60}\text{Co}$  source are shown in Fig. 31. The signals decay with  $4\text{-}\mu\text{s}$  time constant. Although modification of the value of the pole-zero cancellation circuit changes the decay constant, the change is compensated by the pole-zero cancellation digital filter. No fatal errors are found in the oscilloscope and

<sup>4</sup>Bayonet Neill-Concelman

<sup>5</sup>LEMO cable is product of LEMO S.A.

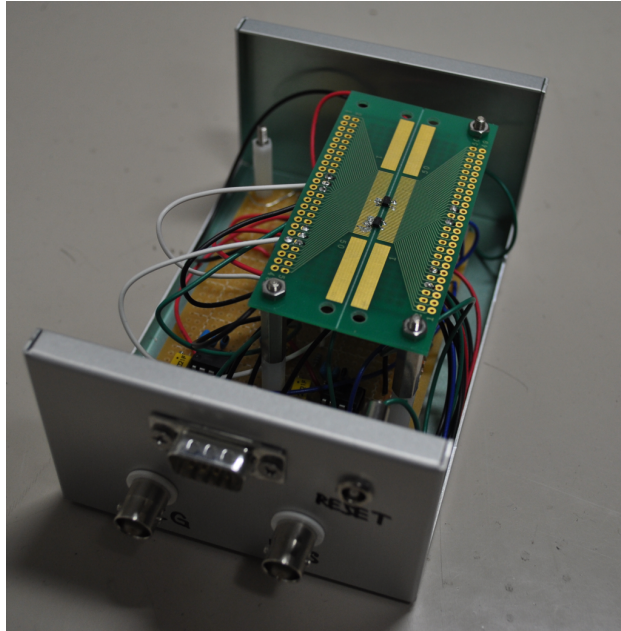


Figure 30: The interface-amp for Techno-AP module.

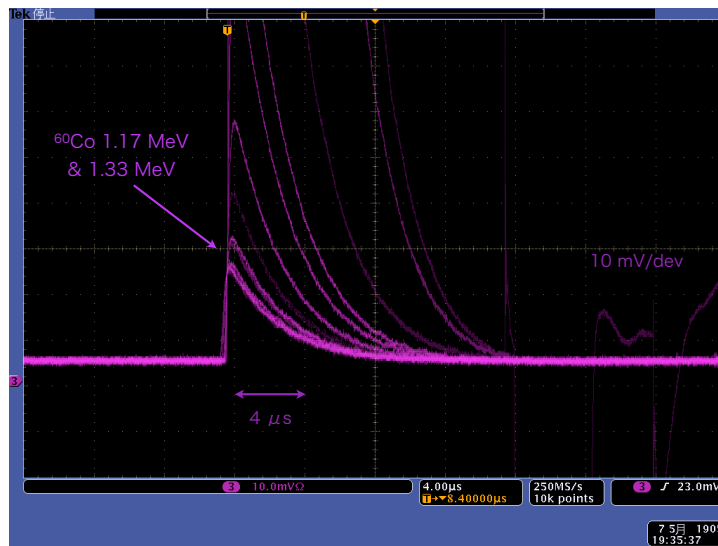


Figure 31: Output from interface-amp. Peaks of <sup>60</sup>Co are shown.

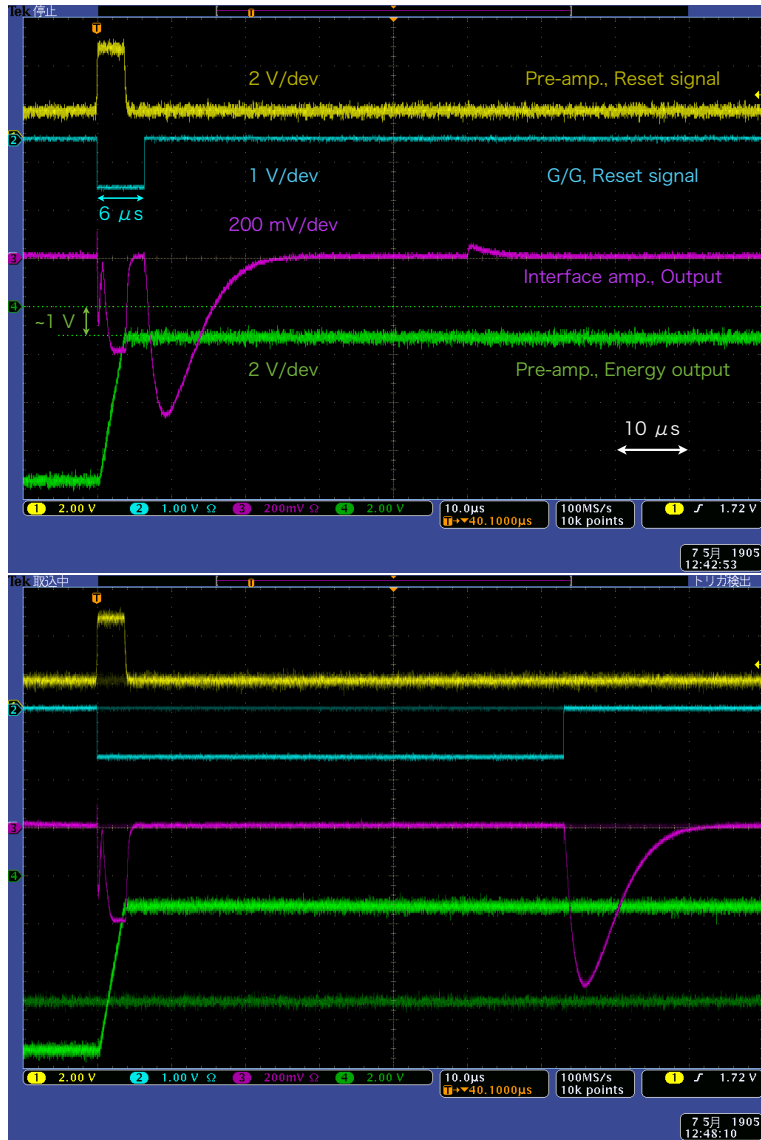


Figure 32: Behavior around the reset signal. Time scale is  $10 \mu\text{s}/\text{dev}$  (white). Arrows on left side are the ground positions. The top (yellow), second (light blue), third (purple) and bottom (green) lines are reset pulses from a Ge detector, the adjusted reset pulse for the interface-amp for Techno-AP module, the output of the interface-amp and signal from the Ge detector, respectively. The width of the reset pulse for the interface-amp on the top figure is set to  $6 \mu\text{s}$  and that of the bottom to  $63 \mu\text{s}$ . Scale of both figures is the same.

pick-up noises are reduced by using an automatic voltage regulator (AVR). The analog full range of DSP is  $\pm 1$  V, and it is one tens of that of PHADC (AD 413A) which has been used for the previous experiments. Furthermore, DSP does not have a noise filter like shaping-amps. Therefore a low noise environment becomes indispensable.

Behavior of the system around the reset signal is shown in Fig. 32. The time scale and voltage scales of each signal are the same for the two figures. The width of the reset pulse for the interface-amp on the top figure is set to  $6 \mu\text{s}$  and that of the bottom to be  $63 \mu\text{s}$ . The width of the white arrow shows  $10 \mu\text{s}$ . In the oscilloscope, the waveforms are acquired via DC coupling and the markers on the left side represent position of the ground level. The top (yellow), second (light blue), third (purple) and bottom (green) lines are reset pulses from a Ge detector, the adjusted reset pulse for the interface-amp, the output of the interface-amp and signal from the Ge detector, respectively. The adjusted reset pulse is NIM signal (Nuclear Instrumentation Module standard) and it is actually converted to TTL signal.

The output of the interface-amp (purple) approaches the ground level in less than  $2 \mu\text{s}$  during the reset. It is confirmed that the fast discharge circuit for the reset itself works as expected. The problem is a stray pulse whose pulse height is  $\sim 600$  mV after the switch turned off in both cases.

The stray phenomena are caused by both the circuit configuration and the DC offset of the input signal. In respect to the circuit configuration, the voltage level of the connection between  $VR$  and  $R1$  ( $C1$  and  $C2$ ) *i.e.*  $V_a$  in Fig. 27 is  $66\%$  ( $= R1/(R1 + VR)$ ) of the input DC component. The Ge detector (ORTEC) outputs the  $\sim -1$  V offset (Fig. 32). The DC component was not considered in the design phase and have to be zero in a normal situation. During the switch engaged,  $V_a$  is almost 1 V because the value of the protective resistance ( $R = 51 \Omega$ ) is much smaller than that of the first filter resistance ( $R1 = 2 \text{ k}\Omega$ ). When the switch is unengaged,  $V_a$  transits from the 1V to the  $66\%$  of the 1V or 660 mV with the time constant of  $C2 \times R2 = 6.8 \mu\text{s}$ . The filter outputs a pulse of the transition. The observed pulse height and the decay constant of the stray pulse agreed with the above discussion, and the behavior of the circuit is confirmed by simulations.

The solutions for the stray pulse are to adjust DC level of the pre-amp. to the ground level and to cut DC component by AC coupling. The DC offsets of pre-amps. are  $\sim 1$  V (ORTEC) and  $\sim 2$  V (CANBERRA), respectively. Figure 33 shows the outputs of reset signals of both pre-amps., schematically. The DC offset cannot be reduced unless modifying the pre-amp., but the

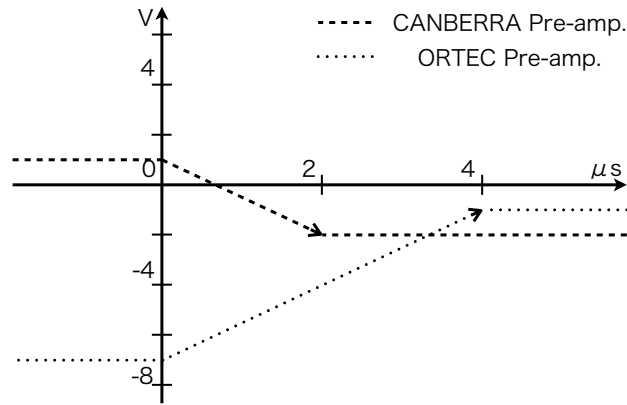


Figure 33: Schematic view of reset output signals of both ORTEC (dotted line) and CANBERRA (dashed line) pre-amp.

modification is not realistic. Therefore, an even-order filter with a pole-zero cancellation feedback at the first capacitor ( $C1$ ) is not usable for the E13 experiments. The odd-order circuits or even-order filters with the feedback on the next capacitor ( $C2$  in this configuration) are able to cut DC component and the stray pulse. In the case of designing odd-order circuits, the switch has to be inserted in the first order circuit which is configured at the entrance of the higher order filter in order to shorten processing time.

#### 4.4.2 The Interface Amplifier for GRETINA Module

Behavior of Tohoku-POB around the reset pulse is displayed in Fig. 34. The width of the bottom black arrow shows  $4 \mu\text{s}$ . The top (light blue), center (purple) and bottom (blue) lines are the pre-amp output, the Tohoku-POB output and the reset trigger signal (TTL), respectively.

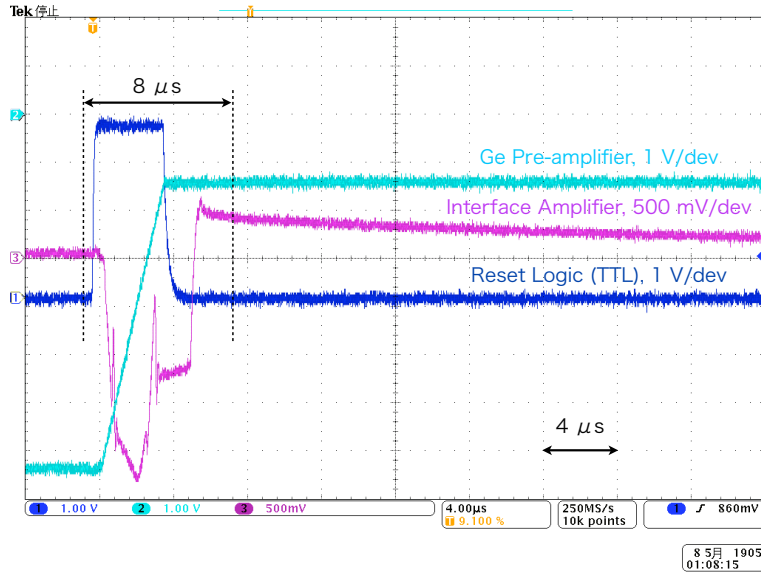


Figure 34: Behaviors around the reset signal. Time scale is  $4 \mu\text{s}/\text{dev}$  (black arrow). Pointers on left side are the ground positions. The top (light blue), center (purple) and bottom (blue) lines are the pre-amp output, the Tohoku-POB output and the reset logic signal, respectively.

The pre-amp. output has also  $\sim 1 \text{ V}$  offset. However, Tohoku-POB has no stray pulse like the second order filter because the pole-zero cancellation feed-back is not installed. The output of Tohoku-POB has  $\sim 500 \text{ mV}$  overshoot after the switch turned off automatically. This is considered to be due to inrush current from the diode to the signal line. The current is discharged by the capacitor and the resistor with  $50\text{-}\mu\text{s}$  time constant. The signal on the shifted baseline can be extracted by the waveform analysis inside the DSP. The dead time is predicted to be  $\sim 8 \mu\text{s}$ , being more  $2 \mu\text{s}$  longer than the required period.

Although the  $\gamma$ -ray signal is analyzed, a circuit with lower shift has a

wider full range after the reset, less dead time and more stable than the developed circuit. The signal during the reset first goes to  $-2.5$  V and then step up to  $-1.5$  V and lastly overshoots. Behavior of the signal is thought to be due to the low bandwidth capability and the threshold voltage of the diode. Since the ideal diode cannot be obtained, the relation between bandwidth of OP-amp and overshoot are investigated. The existence of the inrush current is confirmed by simulation with 10-MHz bandwidth OP-amps., but the high level overshoot cannot be confirmed. Simulation with the ideal OP-amp and an actual diode model has no overshoot hence it is found that the use of wider bandwidth OP-amps than LF356 reduces the overshoot. The use of an OP-amp. with a bandwidth which is several ten times that of a input signal is recommended for the ideal diode circuit. Therefore, an OP-amp. with over 500 MHz bandwidth and voltage feedback type may reduce the overshoot because the bandwidth of the reset signal is  $\sim 10$  MHz. The system has an potential to reduce the dead time to  $6 \mu\text{s}$  by improving the above problems.

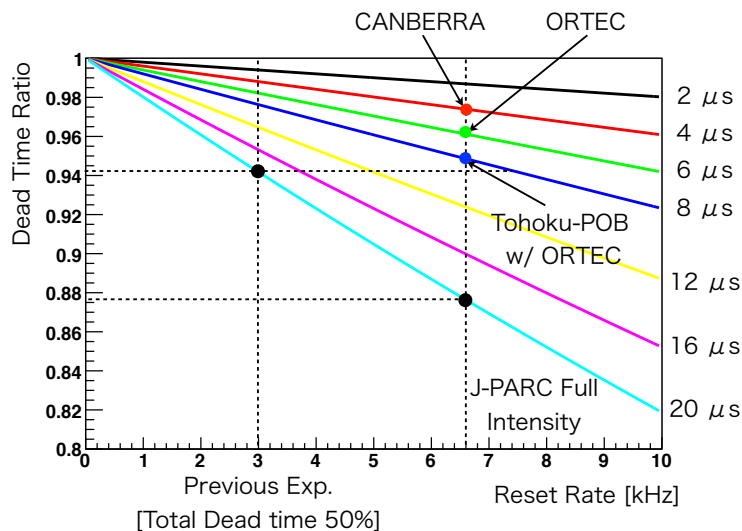


Figure 35: Relation between reset rate and dead time.

Figure 35 shows relationship between reset rate and dead time. The reset rate was almost 3 kHz and the total dead time was  $\sim 50$  % in the previous experiments. Even  $8\text{-}\mu\text{s}$  dead time is comparable to that of the previous condition ( $20 \mu\text{s}$  dead time and 3 kHz reset rate), and handles up to

$\sim 7.5$ -kHz reset rate which is higher than that of the full intensity beam at J-PARC. The total DAQ efficiency is also improved by the use of DSP which converts and transmits data faster than the conventional system. However, more efficient system can improve the quality of data and handle more severe condition. Fortunately, it is found that the goal of  $((\text{reset time}) + 2) \mu\text{s}$  is achievable by the above discussion. Moreover, the first-order filter circuit can also be used with the conventional system by connecting it in front of the shaping-amp to reduce the dead time. Therefore, improved version of interface-amp. for the fast readout can be designed.

## 5 Future Plan

An updated version of Tohoku-POB is being designed for the actual use of the interface-amp. An AC-coupled second-order filter is designed for the fast readout and for the low-frequency noise reduction. A pole-zero cancellation feedback is installed in parallel with a capacitor of a second differentiation circuits. The configuration avoids the stray pulse discussed in Section 4.4. In this section the design of the modified version is overviewed.

The updated version consists of two parts of a signal line and a trigger line. The signal line processes input signal for DSP readout and the trigger line monitors penetrations of charged particles and reset pulses. The schematic diagrams of updated Tohoku-POB, especially a signal line and a trigger line, are shown in Fig. 36 and Fig. 37, respectively.

The signal line consists of input buffers, a second-order high-pass filter, a gain adjustment buffer and a differential amplifier. For simplicity, the input buffer for negative input and the high-pass filter part, namely, the most important part in Tohoku-POB, are drawn in Fig. 36. The non-invert buffer is also installed at the entrance of the signal line for the charged particle trigger. Both the input buffer for positive input and the gain adjustment buffer are shown in Fig. 27. The configuration of the differential output amplifier (AD8132, AD) is the same as that in Fig. 25.

Since the board is operated with GRETINA module at present, an anti-alias filter (low pass-filter) has to be installed. Bandwidth of OP-amps are used as the low-pass filter. The idea reduces the number of implemented elements and hence the distortion of the frequency component especially high frequency component around a few tens mega-hertz order. Total three LF356 amplifiers are inserted in series for the filter. The total gain at 50 MHz is  $\sim -60$  dB ( $\times 0.001$ ).

The Sallen-Key architecture is chosen for the second-order filter. The gain is set to unity. The time constant and corner frequency of the filter is  $4.16 \mu\text{s}$  and  $38.3$  kHz, respectively. The time constant is set to longer than that of Techno-AP module ( $2.2 \mu\text{s}$ ) because a shorter time constant filter is more sensitive to high frequency external noise but Tohoku-POB is separated from DSP and there is more chance to pick up external noise. The value of resistance for the pole-zero cancellation feedback is same to that of the first differentiation circuit *i.e.*  $3 \text{ k}\Omega$ . The amplifier is designed to be used with only transistor reset pre-amps. The switches are inserted from a connection point of C1, C2 and R1 and that of C2, R1 and R2 to the ground. Alignment

of the first switch is changed from the previous filter and solves the 5.5-V limitation of the input amplitude. The configuration enables the first buffer to amplify the signal higher than the previous one and improves the signal to noise ratio.

The updated version also has the charged particle monitoring system. Since the amplifier gain is adjusted so that the highest  $\gamma$ -ray energy of 8 MeV corresponds to the full range of sampling-ADC of  $\pm 1$  V, the energy deposit by charged particle penetrations overflows the acceptable range. The penetration signal takes longer process time than the  $\gamma$ -ray signal because of the higher energy deposit. The reset (discharge) of the charged particle signal is strongly recommended in our experiments. A threshold voltage has to be set in order for the monitoring system to discriminate charged particle penetration events from  $\gamma$ -ray signals. It was confirmed in Section 4.4 that the transistor reset signal of the second filter itself approaches to the ground in less than  $2 \mu\text{s}$  in the case of using TS5A3166 (Fig. 32). Therefore the switches are chosen in this design. The discharging time is set to  $\sim 2 \mu\text{s}$  which is  $1 \mu\text{s}$  shorter than the reset time of ORTEC 973U ( $3 \mu\text{s}$ ). Schematic diagram is drawn in Fig. 37.

The monitoring system consists of the second filter with a short time constant and a comparator. The time constant of the fast filter is  $2.26 \mu\text{s}$ . The default threshold is set to 490 mV and this corresponds to  $\sim 20$  MeV in this configuration. The fluctuation of signal height due to the difference of the charge collection get bigger with shorter time constant than the set value, and the monitoring system get not to detect every charged particle penetration. When a charged particle deposits energy more than 20 MeV in the detector, a comparator (LM311/111, TI) outputs TTL "true" signal. A flip-flop circuit (74ALS74) is configured like Fig. 25, if necessary. The flip-flop is inserted between the comparator and an OR logic integrated circuit. The OR logic (7424/7432 series) is used for gathering the charged particle discharge logic and the transistor reset logic signals. The logic gate of 7424 series has a hysteresis (Schmitt trigger) and that of 7432 series does not have. It is better to use an OR logic gate with hysteresis for our purpose because of a reduction of an influence by noise in the case of the penetration with  $\sim 20$ -MeV energy deposit. It is also comparable to make a comparator with a hysteresis in order not to be influenced by the noise and keep longer the on-stage.

The shutdown circuit for the transistor reset of the pre-amp. can be implemented by using the diode circuit or the SPST switch with an internal

monitoring trigger or an external trigger. Since the shutdown switches are already installed in this design, these can be used commonly. The simplest way is using the external trigger but it has a possibility of deterioration in resolution because of the ground loop between the external trigger line and the signal line. The internal trigger circuit is made from circuit in Fig.25. In this time the external trigger is used without hesitation because a G/G sets precise gate length and it is another difficult problem for the internal resistive feedback timer. Capacitors in the charged particle monitoring system have to be also discharged during the reset signal. The alignment of the switches is the same as that of the main signal line in Fig. 36.

The E24 or E96 elements have to be chosen for the second-order high-pass filter in the signal line and another section in the actual use test. The power for the interface-amps is supplied from NIM crates now and noise contaminates from a power supply line. It is of course better in aspect of the noise reduction to shorten the line and place the modules as close to each other as we can. The earth for the interface-amp. has to be well grounded because the circuit is shorted during the transistor reset or the charged particle penetration. The D-sub connection which is used at present is not well shielded. Furthermore the total thirty two interface-amps. will be used for the experiments. An interface-amp. which can be inserted into a NIM crate is better for our purpose. Four interface-amps. in a module is practical configuration. In this condition, one module for CANBERRA detectors and seven modules for ORTEC detectors are needed. BNC for the input and the D-sub output for GRETINA module are necessary.

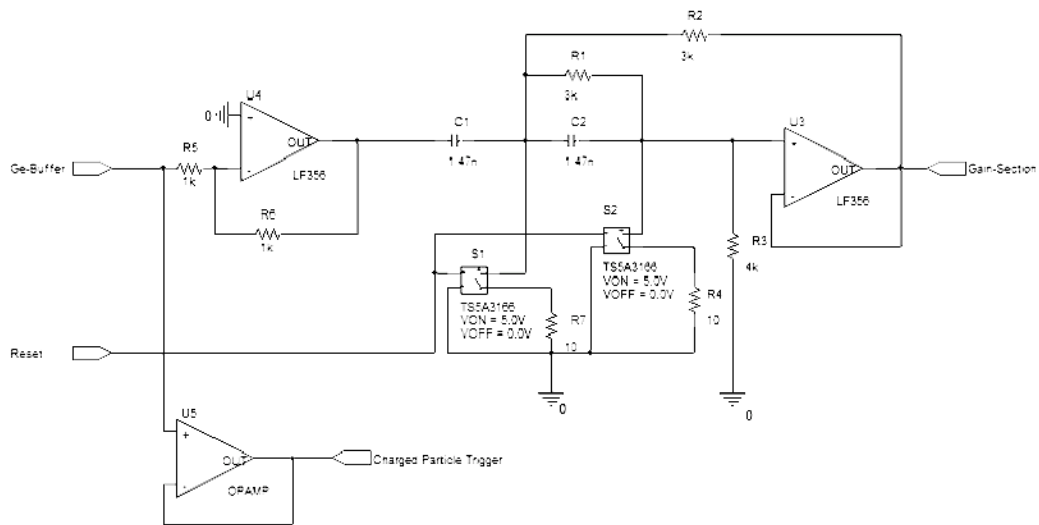


Figure 36: Schematic of signal line of Prototype IA for HBJ.

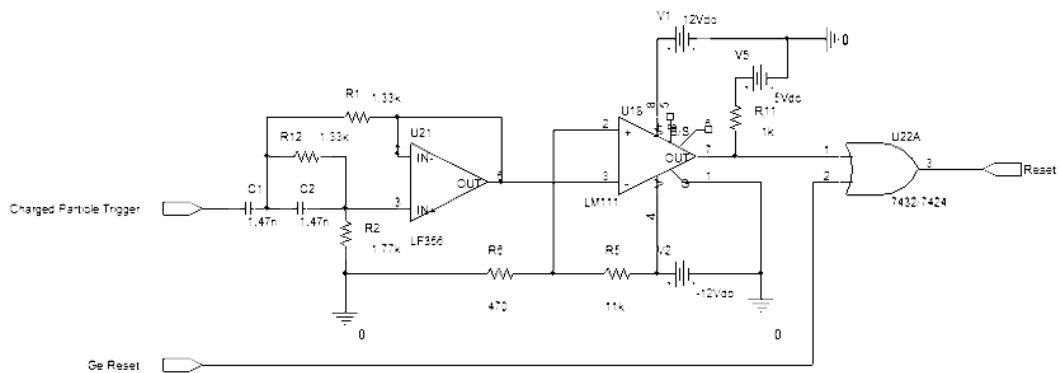


Figure 37: Schematic of reset line of Prototype IA for HBJ.

## 6 Summary

We attempt to perform  $\gamma$ -ray spectroscopy of light hypernuclei by using a detector system, Hyperball-J, at J-PARC. Our experiment is named to E13. We research  $\Lambda$  spin-dependent interaction through the hypernuclear  $\gamma$ -ray spectroscopy with Ge detectors. High resolution (3 keV @ 1.3 MeV of  $\gamma$  ray) of Ge detector enables us to research the interaction because the energy spacing which corresponds to the interaction is a few hundreds keV order and the value is less than the energy resolution of the reaction spectroscopy. We also study another properties of nucleons (charge braking effect between a proton and a neutron, etc.) by using a  $\Lambda$  in a hypernucleus as a probe.

Hyperball-J consists of Ge detectors and background (Compton) suppression counters. The Ge detectors are specialized to the hypernuclear  $\gamma$ -ray spectroscopy. All pre-amplifiers in the Ge detectors for Hyperball-J have a low gain (several tens mV per MeV) and are of transistor reset type because the detectors are exposed to high energy deposit rate ( $\sim 1$  TeV/s) from penetration of charged particles. It is predicted that the conventional readout system can not handle Ge detector signals under the maximum beam intensity ( $\sim 10$  MHz). In order to operate Hyperball-J under severe conditions, the new readout system is necessary.

A new readout system for the low-gain reset type pre-amp of Ge detector is designed. It is found that the system which consists of an interface amplifier and DSP are best way for our experimental condition through the study. DSP with an interface amplifier showed comparable performance with the conventional system. However the interface amplifier generated comparable dead time with the conventional system. Therefore interface amplifiers were newly designed for the reduction of the dominant dead time after reset. It is found that a switching circuit reduces the dead time effectively. The goal dead time is set to 6  $\mu$ s (ORTEC Ge detector) and 4  $\mu$ s (CANBERRA Ge detector). These dead times contain the stabilization time of the circuit.

The interface amplifier was designed by modifying POB at ANL. The interface amplifier with first-order high-pass filter (Tohoku-POB) reduced dead time to 8  $\mu$ s with ORTEC Ge detector and it has yet room for improvement. The amplifier with second-order high-pass filter achieved the goal dead time, but had a stray pulse when the switch unengaged. It was confirmed by circuit simulations that the pulse can be cancelled by changing the alignments of pole-zero cancellation circuit and the amplifier AC-coupled. An updated version of interface amplifier is being also designed for the actual use. The

updated version also resets an input signal when a charged particle penetrates the Ge detector. The system protects circuits in DSP and reduces dead time by the particles. It is predicted that the dead time will be less than  $6 \mu\text{s}$  (ORTEC Ge detector) or  $4 \mu\text{s}$  (CANBERRA Ge detector) after the reset and  $2 \mu\text{s}$  in the case of charged particle penetration.

## 7 Acknowledgement

The author of this master's thesis great thanks to Yoshida Scholarship Foundation (YSF) for financial aid during the master course. The foundation also gave me a chance to meet and discuss about our research with who are the member of the foundation. The financial aid gave me much time to research and I have eventually finish the study.

I would like to write a special thanks to professor H.Tamura for giving me the research subject and for the correction of this master's thesis. The subject was very difficult for me but I could get lots of sense about the experiments and electric circuit. I feel strongly that the experience during the master courses will become one of the most important ones for the academic life.

I address my thanks to P.Wilt for the discussion and lots of help about the design of the interface amplifier. His help is most important factor for the research.

I thank to N.Chiga for teaching me about electric circuit and transistors. His teach enables me to analyze the conventional shaping amplifier, and to develop the interface amplifiers.

I appreciate T.Koike and K.Hosomi for the teach about the physics, Ge detector and readout system.

I also thank to member of CNS, especially S.Shimoura, E.Ideguchi and S.Mitimasa, for the discussion of our experiment and of DSPs.

I address special thanks to acknowledgement professor S.N.Nakamura who taught me physics and English during bachelor course and master courses. Especially he taught me the importance of DAQ and measurement.

I also thank to T.Kawakatsu for the discussion about nuclear science and soft matter physics. Discussions about soft matter physics and engineering gave me lots of idea about the design of the interface amplifier and an thought that wide vision efficiently accelerates development speed.

I appreciate staffs in our lab., my colleagues, S.Hirose, K.Makabe and T.Yamada and M1 students for discussion about our research. I hope their more success in the future.

I personally thanks to H.Li and his family for the discussion about not only physics, experiments but also problems around far east, etc. I could learn lots of way of thinking through his study at Tohoku university. Xiexie!

Lastly, I great thanks to my family for encouraging me about writing theses and researches, especially after the earth quake on 11th March 2011 and help about my life, and also thank to antecedents for having run the

previous Tohoku university during the Edo period. I'm very glad to study and research at the school of Sendai-han in the era of Heisei.

## A Sallen-Key Architecture

Sallen-key architecture is one of second order active filters, and is characterized for its simplicity. The architecture is often selected in the case of unity gain, using reasonable values of capacitances and simple implementation.

Figure 38 shows a schematic diagram of the general Sallen-Key architecture. The gain is set to unity. The analysis of the architecture is based on the assumption that the OP-amp. is ideal.

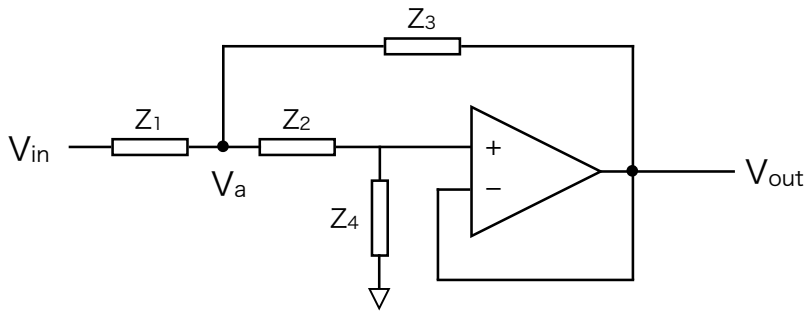


Figure 38: Diagram of the general Sallen-Key architecture with unity gain.

Inputs of OP-amp. are set to be equal each other ( $v_+ = v_-$ ). Furthermore, the inverting input ( $v_-$ ) is fed-back to the output ( $v_{out}$ ) directly, these values are equal, *i.e.*

$$v_+ = v_- = v_{out} \quad (6)$$

By Kirchoff's circuit law (KCL) at the  $v_a$  node,

$$\frac{v_{in} - v_a}{Z_1} = \frac{v_a - v_{out}}{Z_3} + \frac{v_a - v_+}{Z_2}. \quad (7)$$

Combining Eqs. (6) and (7),

$$\frac{v_{in} - v_a}{Z_1} = \frac{v_a - v_{out}}{Z_3} + \frac{v_a - v_{out}}{Z_2}. \quad (8)$$

Applying Eq. 6 and KCL at the non-inverting input ( $v_+$ ),

$$\frac{v_a - v_{out}}{Z_2} = \frac{v_{out}}{Z_4}, \quad (9)$$

which is arranged to

$$v_a = v_{out} \left( \frac{Z_2}{Z_4} + 1 \right). \quad (10)$$

Combining Eqs. (8) and (10),

$$\frac{v_{in} - v_{out} \left( \frac{Z_2}{Z_4} + 1 \right)}{Z_1} = \frac{v_{out} \left( \frac{Z_2}{Z_4} + 1 \right) - v_{out}}{Z_3} + \frac{v_{out} \left( \frac{Z_2}{Z_4} + 1 \right) - v_{out}}{Z_2}. \quad (11)$$

Rearranging Eq. 11 gives the transfer function of the architecture, *i.e.*

$$\frac{v_{out}}{v_{in}} = \frac{Z_3 Z_4}{Z_1 Z_2 + Z_3 (Z_1 + Z_2) + Z_3 Z_4} \quad (12)$$

In the case of a high-pass filter, values of the impedances are

$$Z_1 = \frac{1}{sC_1}, Z_2 = \frac{1}{sC_2}, Z_3 = R_1 \text{ and } Z_4 = R_2, \quad (13)$$

where  $s = j\omega = (\sqrt{-1})2\pi f$ , and  $f$  is a frequency of a pure sinusoidal input. The transfer function is

$$H(s) = \frac{s^2}{s^2 + (2\pi f_0/Q)s + (2\pi f_0)^2} \quad (14)$$

where  $f_0$  and  $Q$  are the cut-off frequency and the quality factor of the filter, respectively. These values are described as

$$f_0 = \frac{1}{2\pi\sqrt{C_1 C_2 R_1 R_2}} \quad (15)$$

$$Q = \frac{\sqrt{C_1 C_2 R_1 R_2}}{R_1 (C_1 + C_2)} \quad (16)$$

The filter cut lower frequency than  $f_0$  with -20 dB/dec. The quality factor ( $Q$ ) is a factor of stability against an oscillation. The quality factor of a Bessel filter is set to  $Q = 1/\sqrt{3}$ .

In the development, the cut-off frequency is changed from above relation because the pole zero cancellation (PZC) feedback is inserted. As described Section 4 (in the second order filter), firstly parameters are calculated by using Eqs. 15 and 16, and then PZCs are inserted. In the case of setting PZC analytically, the transfer functions between  $v_{in}$  and  $v_a$  and between  $v_a$  and  $v_{out}$  are needed. These relations are calculated by using Eqs. 8 and 10.

## B Pole-Zero Cancellation Feedback

In the nuclear and particle physics experiments, a pole-zero cancellation feedback (PZC) is often implemented in a shaping amplifier. Effects of PZC are to prevent undershoot of processed signal and to shorten decay time constant of a pre-amplifier whose decay time is normally set to several hundred microseconds due to noise reduction. The function of PZC is briefly analyzed in this appendix.

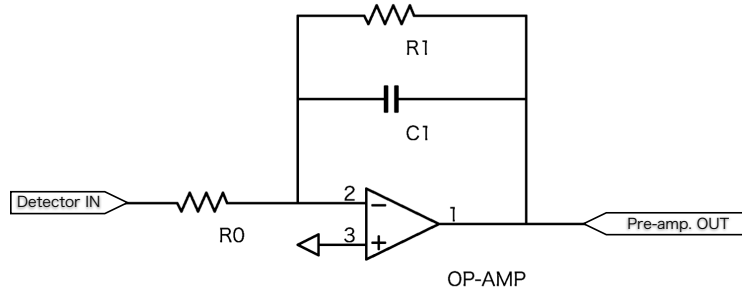


Figure 39: Diagram of a charge sensitive pre-amplifier with resistive feedback.

Figure 39 shows schematic diagram of charge sensitive pre-amplifier. This is a kind of inverting amplifier. The in-coming charge is stored in capacitor  $C_1$ , and is discharged via resistor  $R_1$  to restore the base line. The transfer function is calculated by considering KCL and relation of non-inverting and inverting inputs ( $v_+ = v_-$ );

$$H_1(s) = -\frac{1}{R_0} \frac{R_1}{1 + sC_1R_1} \quad (17)$$

The time constant of  $C_1R_1$  is set to several ten micro second in order to prevent the deterioration of resolution and of rise time of input signal.

Figure 40 shows circuit diagram of PZC feedback. The transfer function of PZC is described as follows:

$$H_2(s) = \frac{R_3}{R_2 + R_3} \frac{1 + sC_2R_2}{1 + sC_2(R_2||R_3)} \quad (18)$$

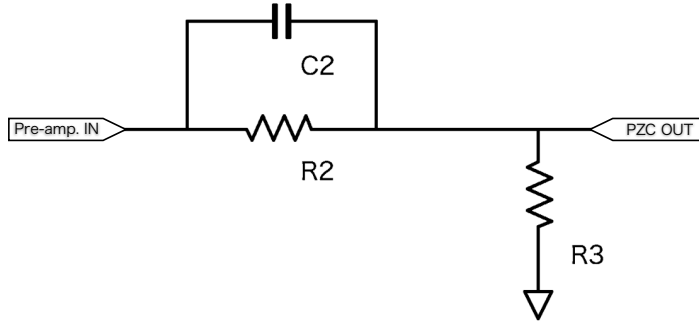


Figure 40: Diagram of a pole-zero cancellation feedback.

Setting  $C_2R_2 = C_1R_1$ , the zero of  $H_2$  compensates the pole of  $H_1$ , which is the reason of calling PZC. The function of PZC is to shorten the decay constant of pre-amplifier ( $C_1R_1$ ) down to  $C_2(R_2||R_3)$ , and to prevent undershoot of processed signal in shaping amplifier section.

In this development, only the second order filters (Figs. 27 and 36) need PZC feedback because a pre-amplifier of Ge detector for HBJ does not have a differentiation feedback. It is considered that the first differentiation section in the second order filters corresponds to the discharge feedback of the pre-amp. Therefore, PZC feedback is inserted in order to compensate the other pole, in the case of Fig. 36, the value of PZC ( $C_2R_1$ ) is set to  $C_1R_2$ .

## References

- [1] O.Hashimoto and H.Tamura, Spectroscopy of  $\Lambda$  hypernuclei, Elsevier, 2004.
- [2] H. Tamura, et al.; Gamma-ray spectroscopy of light hypernuclei; J-PARC proposal E13, 2006.
- [3] K.Hosomi, Development of waveform readout method for Ge detector, Master's thesis, Tohoku univ., 2007.
- [4] Data sheet of ORTEC 671 spectroscopy amplifier, AMETEK.
- [5] Data sheet of ORTEC 973U Ultra-High-Rate spectroscopy amplifier, AMETEK.
- [6] Data sheet of ORTEC AD413A CAMAC quad 8k ADC, AMETEK.
- [7] Data sheet of TS5A3166 0.9- $\Omega$  SPST analog switch, TI., 2005.
- [8] Data sheet of SN74ALS74A, dual positive-edge-triggered D-type flip-flops with clear and preset, TI., 1982.
- [9] Data sheet of LF356 JFET input operational amplifiers, TI, 2001.
- [10] Data sheet of LM311 voltage comparator, TI, 2001.
- [11] Application report, Analysis of the Sallen-Key Architecture, TI, 2002.
- [12] Data sheet of AD8132 low cost, high speed differential amplifier, AD.
- [13] DSP (digital signal processing) hardware manual, Techno-AP, 2011.
- [14] DSP (digital signal processing) software manual, Techno-AP, 2011.